European Journal of Pharmacology 985 (2024) 177087

Contents lists available at ScienceDirect

European Journal of Pharmacology

journal homepage: www.elsevier.com/locate/ejphar

Are we better together? Addressing a combined treatment of pitavastatin and temozolomide for brain cancer

João Basso [a,b], Ana Miguel Matos [a,c], Saeid Ghavami [d,e,f], Ana Fortuna [a,g], Rui Vitorino [h,i], Carla Vitorino [a,b,*]

[a] Faculty of Pharmacy, University of Coimbra, Coimbra, Portugal
[b] Coimbra Chemistry Centre, Institute of Molecular Sciences—IMS, Faculty of Sciences and Technology, University of Coimbra, Coimbra, Portugal
[c] Chemical Engineering and Renewable Resources for Sustainability, CERES, Faculty of Pharmacy, University of Coimbra, Coimbra, Portugal
[d] Department of Human Anatomy and Cell Science, University of Manitoba College of Medicine, Winnipeg, MB, R3E 0J9, Canada
[e] Research Institute of Oncology and Hematology, Cancer Care Manitoba-University of Manitoba, Winnipeg, MB, R3E 0V9, Canada
[f] Biology of Breathing Theme, Children Hospital Research Institute of Manitoba, University of Manitoba, Winnipeg, MB, R3T 2N2, Canada
[g] Coimbra Institute for Biomedical Imaging and Translational Research, University of Coimbra, Coimbra, Portugal
[h] Department of Medical Sciences, Institute of Biomedicine-iBiMED, University of Aveiro, Aveiro, Portugal
[i] UnIC@RISE, Department of Surgery and Physiology, Faculty of Medicine of the University of Porto, Porto, Portugal

ARTICLE INFO

Keywords:
Glioblastoma
Mevalonate pathway
Proteomics
Spheroids
Synergism

ABSTRACT

Pitavastatin is commonly prescribed to treat hypercholesterolemia through the regulation of cholesterol biosynthesis. Interestingly, it has also demonstrated a great potential for treating brain tumors, although the detailed cytotoxic mechanism, particularly in glioblastoma, remains incompletely understood. This work explores the activity of pitavastatin in 2D and 3D glioblastoma models, in an attempt to provide a more representative and robust overview of its anticancer potential in glioblastoma. The results show that not only is pitavastatin 10-1000 times-fold more effective in reducing tumoral metabolic activity than temozolomide, but also demonstrate a synergistic activity with this alkylating drug. In addition, low micromolar concentrations of this statin strongly impair the growth and the invasion ability of multicellular tumor spheroids. The obtained qRT-PCR and proteomics data highlight the modulation of cell death via apoptosis (*BAX/BCL2, CASP9*) and autophagy (*BECN1, BNIP3*, *BNIP3L* and *LC3B*), as well as an epithelial to mesenchymal transition blockage (HTRA1, SERPINE1, WNT5A, ALDH3B1 and EPHA2) and remodeling of the extracellular matrix (VCAN, SERPINE1 and TGFBI). Overall, these results lay the foundation for further investigations on the potential combinatory clinical treatment with temozolomide.

1. Introduction

Glioblastoma is a grade 4 IDH-wildtype astrocytoma and the most common form of primary brain tumors, representing approximately 60% of all gliomas (Ostrom et al., 2022). Patients diagnosed with this pathology are clinically treated with surgical resection followed by radiotherapy and concomitant/adjuvant temozolomide (approved in 1999), although the two-year survival is limited to 26.5 % (Stupp et al., 2005a). As of today, there are only a few alternatives to the standard of care, which are now being used in recurrent glioblastomas: oral, local or intravenous nitrosoureas (carmustine and lomustine, approved in the 1970s) and bevacizumab (approved in 2010), an antiangiogenic therapy that ultimately shows no benefits in overall survival, although it may improve progression-free survival and cognition (Fu et al., 2023; Kotecha et al., 2023). Glioblastoma was originally categorized into four subtypes, according to different transcriptional signatures on EGFR, NF1, and PDGFRA/IDH1: proneural, neural, classical, and mesenchymal (Verhaak et al., 2010). Yet, a recent analysis reviewed this classification and excluded the neural subtype, attributing it to contamination of the original samples with nontumor cells (Sidaway, 2017; Wang et al., 2017a). Tumor aggressiveness and treatment resistance are commonly observed in the mesenchymal subtype and are frequent in the context of glioblastoma relapse (Wang et al., 2017a), which is credited to tumor heterogeneity and aggressive behavior, as well as to the presence of cancer stem cells and gaining of resistance (Miranda et al., 2017; Stupp et al., 2005a). In fact, the majority of patients develops aggressive

* Corresponding author. Faculty of Pharmacy, University of Coimbra, Coimbra, Portugal.
E-mail address: csvitorino@ff.uc.pt (C. Vitorino).

https://doi.org/10.1016/j.ejphar.2024.177087
Received 13 September 2024; Received in revised form 29 October 2024; Accepted 30 October 2024
Available online 2 November 2024

recurrences 2–3 cm away from the original lesion within the first year after treatment (Rapp et al., 2017; Stupp et al., 2005b; Yan et al., 2009).

The need for providing an effective treatment for glioblastoma has pushed the scientific community into exploring not only new compounds, but also the potential of already approved drugs through a drug repurposing perspective (Basso et al., 2018). Statins are the first line therapy for hypercholesterolemia, as they are 3-hydroxy-3-methylglutaryl coenzyme A (HMG-CoA) reductase inhibitors. The direct blockage of the enzyme's active site leads to the inhibition of the conversion of HMG-CoA to mevalonate, the rate-limiting step in the biosynthesis of cholesterol, which is essential for cancer growth and is intimately linked to autophagy and apoptosis. For additional information on the role of this drug class in cancer, the reader is referred to the following review articles: (Afshari et al., 2021; Alrosan et al., 2023; Jiang et al., 2021).

Previous works from our group showed that simvastatin enhances temozolomide-induced cell death through the inhibition of the autophagic flux, activation of the unfolded protein response pathway and increase in reactive oxygen species with mitochondrial damage and apoptosis (Dastghaib et al., 2020; Hajiahmadi et al., 2023; Shojaei et al., 2018). Similarly, lovastatin in combination with temozolomide impairs the autophagic flux, while atorvastatin displays chemosensitizing properties through the inhibition of Ras prenylation (Peng et al., 2017; Zhu et al., 2019).

Among the different commercialized statins, pitavastatin might show the most promising activity, as it outperformed the remaining ones in a heterotopic mice model of glioblastoma (Jiang et al., 2014a). In addition, it shows a potential for combination therapy due to its high lipophilicity, which facilitates cell membrane penetration and a more effective intracellular activity. It also shows favorable pharmacokinetics with a long half-life time, good oral bioavailability and potential to cross the blood-brain barrier.

There are a few clinical trials focusing on the application of statins in glioblastoma, in monotherapy or in combination with radiotherapy, temozolomide or other drugs (Alrosan et al., 2023; Rendon et al., 2022). These include one ongoing Phase 0 trial (NCT05977738) that aims at evaluating pitavastatin concentration at post resected tumors. In fact, further non-clinical and clinical studies are needed to confirm, not only its ability to reach cytotoxic concentrations within the tumor, but also possible synergistic effects, efficacy and safety in the treatment of glioblastoma.

This work explores the anticancer activity of pitavastatin in 2D and 3D models of glioblastoma and lays a foundation for further investigations on the potential combinatory treatment with temozolomide.

2. Materials and methods

2.1. Materials

2.1.1. Drugs and reagents

Pitavastatin calcium (99.8%, CAS number: 147526-32-7) was kindly offered by the Tecnimede group (Sintra, Portugal), whereas temozolomide (99%, CAS number: 85622-93-1) was purchased from Hangzhou Royall Import & Export Co., Ltd (Hangzhou, China). Water (Ω = 18.2 MΩ cm, TOC <1.5 μg/L) was ultrapurified (Sartorius®, Gottingen, Germany) and filtered through a 0.22 μm nylon filter before use. Stock solutions were prepared in dimethyl sulfoxide (DMSO) before each analysis. Cell culture reagents, specifically, high glucose DMEM, sodium bicarbonate, fetal bovine serum (FBS), trypsin, phosphate buffered saline, resazurin sodium salt and penicillin-streptomycin were procured from Sigma-Aldrich (Saint Louis, WI, USA).

2.1.2. Cell lines and culture conditions

A-172 (ATCC CRL-1620), H4 (ATCC HTB-148), U118-MG (ATCC HTB-15) and U-87 MG (ATCC HTB-14) were acquired from the American Type Culture Collection (ATCC, USA), whereas U-373 MG (Uppsala) was kindly provided by the cell bank of the Centre for Neuroscience and Cell Biology of the University of Coimbra. Cells were subcultured after reaching 70–90% confluence and maintained at low passage number in T75 tissue culture flasks, with complete media containing high glucose DMEM, sodium bicarbonate, 10% FBS and 1% penicillin-streptomycin, incubated under standard conditions (37 °C in a humidified 5 % CO_2 atmosphere). All cell lines were negative for mycoplasma and regularly monitored by optical microscopy for any morphological changes. Three biologically independent experiments and methodological triplicates were done for the analyses.

2.2. Methods

2.2.1. Metabolic activity

Metabolic activity was evaluated through the determination of resazurin reduction to resorufin, by living cells, according to manufacturer's instructions. The experimental conditions of the assay, including the cell line, number of seeded cells and incubation period were firstly optimized. Briefly, 5000 cells (25 000 cells/mL, 200 μL) were seeded in 96 well plates and left to adhere for 24 h. The medium was then removed, and cells treated with different concentrations of pitavastatin or temozolomide for 48 or 72 h. A resazurin 10 X solution (0.1 mg/mL in PBS) was directly added to cells in culture medium, which were further incubated at 37 °C for a predetermined time, depending on the cell line. Metabolic activity was analyzed by UV/Vis spectrophotometry using a BioTek Synergy HT microplate reader (Winooski, EUA) at two wavelengths (570 nm and 600 nm) and normalized according to positive (0 %) and negative controls (100 %). Half maximal inhibitory concentrations (IC_{50}) were determined after plotting metabolic activity in function of drug concentration and defining the non-linear sigmoidal curve fitting.

2.2.2. Drug combination studies

Drug combination studies were conducted according to the Chou-Talalay method (Chou, 2010). U-87 MG cells were seeded in 96 well plates, as described above, and treated with increasing concentrations of pitavastatin, temozolomide and their combination at a fixed dose ratio for 48 or 72 h, corresponding to 0.25, 0.5, 1, 2 and 4 times the individual IC_{50} values of each drug. Note that this method recommends the use of a constant-ratio drug combinations to generate the experimental matrix (Chou, 2010). Furthermore, the rationale for the selection of this concentration range was driven by the need to comprehensively assess the pharmacological interactions between these drugs. As such, the concentrations encompass both lower and higher doses to explore the full scope of potential cellular responses. Metabolic activity was determined as aforementioned. The Combination Index (CI) was calculated in CompuSyn v1.0 (ComboSyn Inc, NY USA), considering that both drugs display independent mechanisms of action. Accordingly, this coefficient describes different pharmacological interactions between two or more drugs: $CI < 1$ (synergism), $CI = 1$ (additive interaction), $1 < CI < 5$ (competition) $CI > 10$ (antagonism). Note that the synergy scale varies from 0 to 1, while the antagonism scale goes up to $+\infty$ (Chou, 2010).

2.2.3. Multicellular tumor spheroid (MCTs) kinetics study

The effect of pitavastatin and temozolomide was tested on 3D spheroid cultures, as described by Vinci and colleagues (Vinci et al., 2012). Briefly, 1000 U-87 MG cells (5000 cells/mL, 200 μL) were seeded into 96-well round-bottomed ultra-low attachment plates (faCellitate GmbH, Germany) and incubated for 4 days at 37 °C, 5 % CO_2 to form spheroids. Images were captured using an inverted microscope, and the mean spheroid Feret's diameter and roundness were determined in ImageJ V.1.54f.

A 50 % media replenishment was performed on days 4, 7, 10, 12 and 14. In addition, spheroids were treated with 100 μL of 2 X pitavastatin, temozolomide or their combination, with a final concentration

corresponding to the respective IC_{50} at 48 h. Growth kinetics was evaluated up to 17 days after cell seeding, at regular intervals. The reproducibility of the assay was determined by measuring the variation of the spheroid size in triplicate of the three independent experiments on day 4 post seeding.

2.2.4. MCTs invasion assay

Standard 12-well plates were coated with rat tail collagen (200 μg/mL) in PBS for 1 h at 37 °C. 4-day old MCTs were carefully transferred to wells prefilled with 1 mL of FBS 2% (v/v) containing different concentrations of pitavastatin, temozolomide and their combination. Note that MCTs were maintained in low serum conditions and treated with low drug concentrations, in order to avoid the observation of proliferative effects. MCTs were left to adhere, and images were captured at 24, 48 and 72 h. Photographs were then processed in ImageJ and the fold change of the invasion area was estimated according to the following equation:

$$Area\ FC = \frac{\Delta Area\ (Total - MCT)}{Area\ Total}$$

2.2.5. Real-time quantitative reverse transcription PCR

The expression levels of different mRNAs involved in apoptosis and autophagy was assessed by real-time quantitative reverse transcription PCR (qRT-PCR) (Magalhães et al., 2022; Rezazadeh et al., 2020). U-87 MG cells (75 000 cells/mL, 2 mL) were seeded in 6 well plates for 24 h, treated with 0.25 × IC_{50} at 48 h of pitavastatin, temozolomide or their combination, and further incubated for 24 h. Total RNA was extracted with 800 μL of NZYol (NZYtech, Lisbon, Portugal) according to the manufacturer's recommendations. Chloroform (160 μL) were added to each sample, vortexed and centrifuged at 12 000 *g* for 15 min at 4 °C. The aqueous phase was then collected, and the RNA precipitated and purified with different centrifugation cycles (12 000 *g*, 5–15 min, 4 °C), using 400 μL of cold isopropyl alcohol and 800 μL of ethanol 75 % (V/V). The RNA was resuspended in RNAse free water and quantified by UV spectrophotometry using a NanoDrop ND-1000 (ThermoFisher Scientific, Wilmington, DE, USA). Purified total RNA (2.5 μg, A260/A280 ≥ 1.9) was reversed transcribed to cDNA using an NZY First-Strand cDNA Synthesis Kit (NZYtech). The reaction was inactivated by heating the samples at 85 °C for 5 min and the RNA degraded by an RNAse H. qRT-PCR was performed on a CFX96 Real-Time PCR Detection System (Bio-Rad Laboratories, Hercules, CA, USA). Briefly, aliquots of 30 ng of cDNA were amplified with NZYSpeedy qPCR Green Master Mix 2X (NZYtech) using the primers of Table S1, Supplementary Material (0.4 μM) and the following conditions: for apoptosis, 2 min at 95 °C, 40 cycles of 5 s at 95 °C, 30 s at 60 °C; for autophagy, 15 min at 95 °C, 40 cycles of 15 s at 95 °C, 15 s at 58 °C and 20 s at 72 °C). Fluorescence was read at the end of each annealing step. After amplification, melting curves were analyzed through increments from 55 to 95 °C (0.5 °C/step for 5 s). Gene expression was analyzed using the cycle threshold (C_T), in Bio-Rad CFX Maestro 1.1 V4.1.2433.1219 (Bio-Rad Laboratories). The results were normalized to GAPDH as the housekeeping gene and expressed in relation to untreated cells ($2^{-\Delta\Delta CT}$), according to the following equation:

$$Relative\ expression = \frac{2^{\Delta C_T(GAPDH-Gene)_{Sample}}}{2^{\Delta C_T(GAPDH-Gene)_{Untreated\ cells}}}$$

2.2.6. Proteomics

For proteomic experiments, 2 x 10^6 U-87 MG cells were seeded in T75 flasks and left to adhere for 24 h. Cells were washed and treated with 25 μM pitavastatin or DMSO in FBS and antibiotic-free DMEM for 24 h. After treatment, cells were washed with PBS and lysed using RIPA with cOmplete™ Protease Inhibitor Cocktail (Sigma) in ice cold conditions. After scrapping, samples were sonicated in an ice bath and centrifuged at 12 000 *g*, 4 °C for 10 min. Total protein in the supernatant was quantified using the DC Protein Assay (Bio-Rad) and interpolated from a bovine serum albumin standard curve.

2.2.6.1. Liquid chromatography tandem mass spectrometry analysis. The identification and quantification of proteins were conducted by nanoLC-MS/MS in an Ultimate 3000 liquid chromatography system coupled to a Q-Exactive Hybrid Quadrupole-Orbitrap mass spectrometer (Thermo Scientific, Bremen, Germany). Each sample (500 ng of peptides) was loaded onto a trapping cartridge Acclaim PepMap C18 100 Å, 5 mm × 300 μm i.d., 160454, Thermo Scientific, Bremen, Germany) with a mobile phase of 2% acetonitrile (ACN) and 0.1% formic acid (FA) at 10 μL/min. Following a 3 min loading period, the trap column was switched in-line to a 50 cm × 75 μm inner diameter EASY-Spray column (ES803, PepMap RSLC, C18, 2 μm, Thermo Scientific, Bremen, Germany) at 250 nL/min. Peptide separation was achieved with 0.1 % FA (A) and 80 % ACN, 0.1 % FA (B) under the following gradient conditions: 5 min (2.5–10 % B), 120 min (10–30 % B), 20 min (30–50 % B), 5 min (50–99 % B) and 10 min (99 % B). The column was then equilibrated with 2.5 % B for 17 min. Data were acquired with Xcalibur 4.0 and Tune 2.9 (Thermo Scientific, Bremen, Germany). The mass spectrometer was controlled in the data-dependent (dd) positive acquisition mode, alternating between a full spectrum scan (m/z 380–1580) and subsequent HCD MS/MS of the top 10 intense peaks from a full scan (normalized collision energy of 27 %), with an ESI spray voltage of 1.9 kV. The global settings were as listed: use lock masses best (m/z 445.12003), lock mass injection Full MS and peak width (FWHM) of 15 s. The full scan settings were as follows: 70 k resolution (m/z 200), AGC target 3 × 10^6, maximum injection time 120 ms; dd settings: minimum AGC target 8 × 10^3, intensity threshold 7.3 × 10^4, charge exclusion: unassigned, 1, 8, >8, peptide match preferred, exclude isotopes on, and dynamic exclusion 45 s. The MS2 settings were as follows: microscans 1, resolution 35 k (m/z 200), AGC target 2 × 10^5, maximum injection time 110 ms, isolation window 2.0 m/z, isolation offset 0.0 m/z, dynamic first mass, and spectrum data type profile.

2.2.6.2. Proteomics data analysis. The raw spectrometry proteomics data were uploaded to MaxQuant (V.2.5.2.0) and MS/MS spectra were compared to the Uniprot FASTA protein sequence database (*Homo sapiens*, release version of February 1, 2023 using Andromeda, with an FDR for identification of 0.1. For that, protein N-term acetylation, deamidation and methionine oxidation as variable modifications and cysteine carbamidomethylation as fixed modification were considered.

A total of 4570 identified proteins were uploaded into Perseus (V.2.0.9.0). Data were initially filtered to remove proteins only identified by site, reverse sequences, and potential contaminants, resulting in 4220 proteins. Data were further reduced to only include proteins with LFQ intensities in each biological replicate, leading to 1936 hits. Note that 51 proteins were solely identified in the three replicates of the control or of the pitavastatin group, but not in both. Differentially expressed proteins between samples were identified after a $\log_2$ transformation, using a two-sided *t*-test with 250 randomizations and an FDR of 0.05. The function of the resulting 298 proteins was further evaluated in STRING V.12.0, taking into consideration their difference relative to the control. Data were also uploaded to MetaboAnalyst V5.0 for biostatistics analysis and visualization purposes, as well as to Cytoscape V3.10.0 and ClueGO V2.5.10 for clustering and gene ontology analyses.

2.2.7. Statistical analysis

Data were processed using GraphPad Prism V8.3.0 (San Diego, CA, USA), unless otherwise stated, and are presented as the mean ± standard deviation (mean ± SD). One-way analysis of variance (ANOVA) with multiple comparisons was used when appropriate. Differences were considered statistically significant when $^*p < 0.05$, $^{**}p < 0.01$, and $^{***}p < 0.001$.

3. Results

3.1. Metabolic activity

The anticancer potential of pitavastatin was evaluated over different types of gliomas, including one neuroglioma and four glioblastoma cell lines. Metabolic activity was measured after a 48 and 72 h treatment with increasing concentrations of pitavastatin (Fig. 1). The Fitting parameters of the nonlinear regressions for metabolic activity determination are presented in Table S2, Supplementary Material. Accordingly, pitavastatin shows a strong effect in decreasing metabolic activity, both time and concentration dependent, with IC_{50} values ranging from 0.66 to 23.81 μM (A-172 < H4 < U-373 MG < U-118 < U-87 MG) at 48 h and 0.29–9.39 μM (A-172 < U-373 MG < U-118 < U-87 MG < H4) at 72h.

Three cell lines, differing on their sensitivity to pitavastatin (A-172 - low, U-373 MG - medium and U-87 MG - high), were also treated with temozolomide. In contrast to the low micromolar concentrations obtained for the statin, glioblastoma cells are intrinsically more resistant to the standard of care, with IC_{50} values ranging from 197 to 639 μM (U-373 MG < U-87 MG < A-172) at 48 h and 144–554 μM (U-373 MG < U-87 MG < A-172) at 72 h. Interestingly, the most sensitive cell line to pitavastatin was the most resistant to temozolomide. Low passage U-87 MG cells were chosen for the next studies, due to their extensive use and characterization, glioblastoma-like behavior, self-assembling ability and *in vivo* tumorigenicity (Basso et al., 2021; Vinci et al., 2012; Wen et al., 2024).

3.2. Pitavastatin and temozolomide combination studies

U-87 MG cells were exposed to a fixed drug ratio corresponding to 0.25, 0.5, 1, 2 and 4 times the individual IC_{50} values previously determined (Section 3.1). According to Fig. S1, Supplementary Material, while pitavastatin and temozolomide dose-effect curves are sigmoidal ($m > 1$), the combination curves follow a flat sigmoidal shape ($m < 1$). In addition, all curves show a great conformity with the mass-action law, as $r > 0.95$.

Overall, increasing concentrations of pitavastatin and temozolomide lead to a decrease in metabolic activity at 48 and 72 h (Fig. 2). Yet, for the highest concentration combinations, 2 and 4 × IC_{50}, there is a significantly higher response, in comparison to cells treated separately ($p < 0.05$). The CIs were determined for each condition and are associated to the effect level (Fa, measured as cell death) according to the Chou-Talalay method (Table S3, Supplementary Material). The simultaneous treatment with pitavastatin and temozolomide results in different pharmacological effects, depending on the combination pair. At 48 h and for the lowest concentration, both drugs display a synergistic effect (CI = 0.64, Fa = 0.41); when using 0.5 × IC_{50}, the pair exhibits a nearly additive effect (CI = 1.04, Fa = 0.52); the remaining combinations are characterized by a competitive/antagonistic interaction (CI = 1.90, Fa = 0.57; CI = 2.85, Fa = 0.72; CI = 3.43, Fa = 0.89). The same behavior is observed for the 72 h treatments.

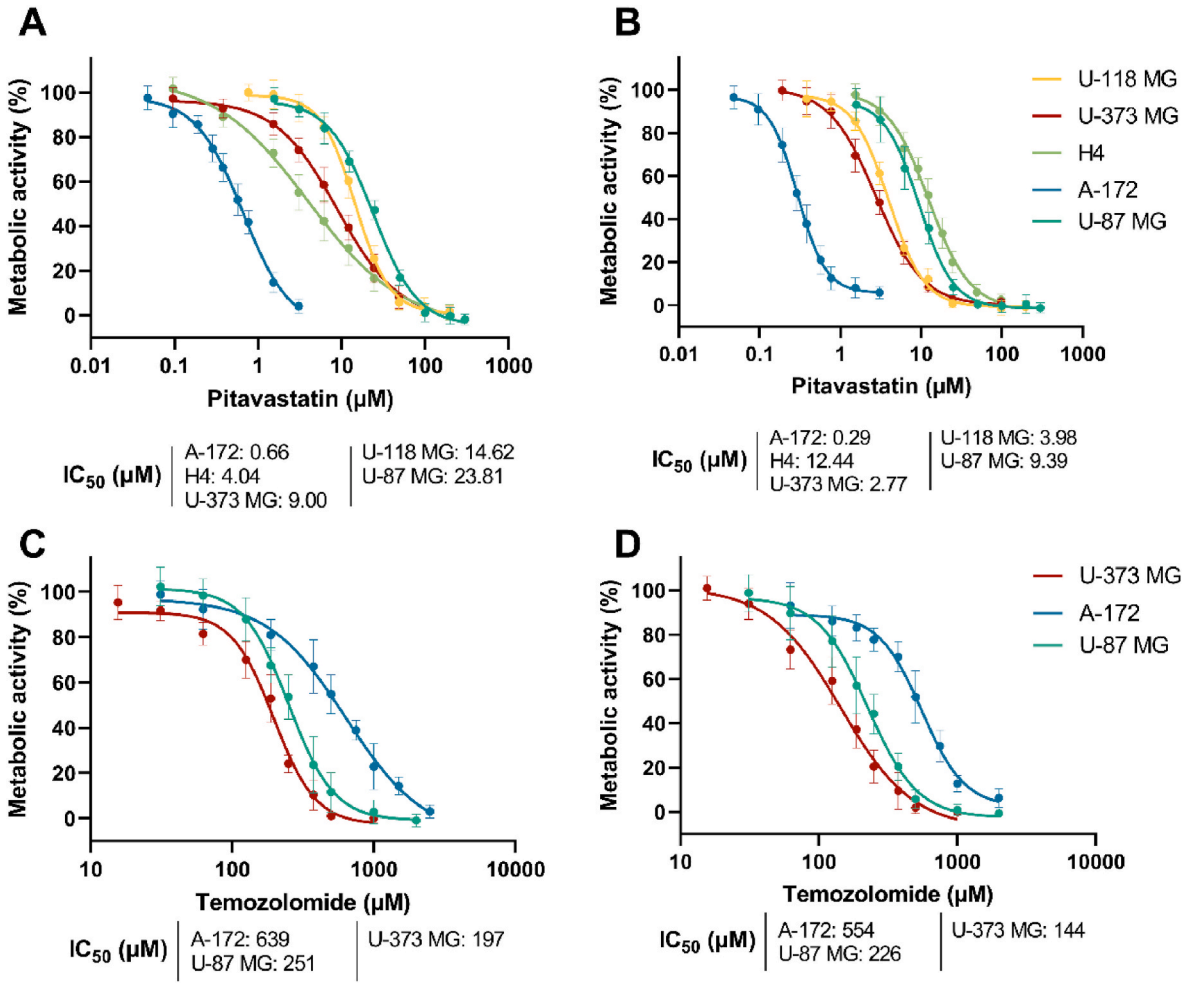

Fig. 1. Dose-effect curves of glioblastoma cells with low, medium and high resistance to pitavastatin, treated with increasing concentrations of temozolomide for 48 h (**A, C**) and 72 h (**B, D**). Metabolic activity was measured by resazurin assay, with IC_{50} values calculated after defining the non-linear sigmoidal curve fitting. Assays were performed in triplicate, in at least three independent experiments, with data being expressed as mean ± standard deviation (SD).

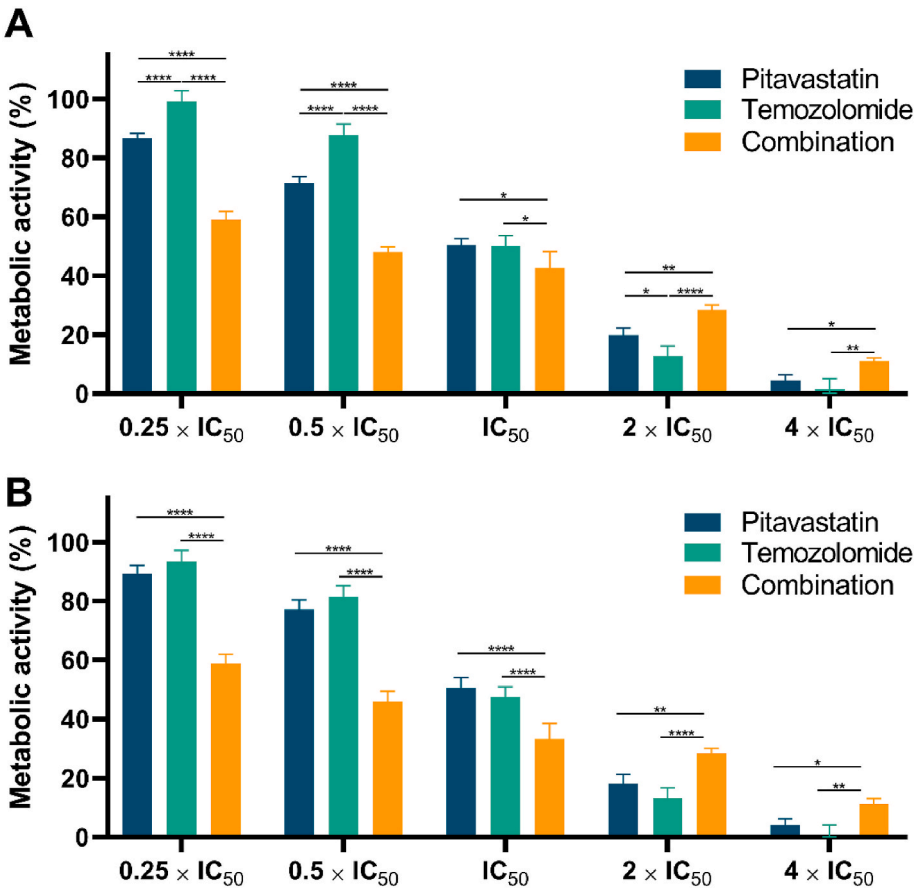

Fig. 2. Dose-response charts of U-87 MG cells after co-treatment with fixed-dose ratios (0.25, 0.5, 1, 2 and 4 times the individual 48/72 h IC_{50} values of pitavastatin and temozolomide) for 48 h (**A**) and 72 h (**B**). Assays were performed in triplicate, in at least three independent experiments, with data being expressed as mean ± SD (one-way ANOVA ($\alpha = 0.05$) with Tukey's multiple comparisons (95% CI); $^{*}p < 0.05$, $^{**}p < 0.01$, $^{***}p < 0.001$, $^{****}p < 0.0001$.

3.3. Multicellular tumor spheroids

3.3.1. Growth kinetics studies

MCTs formed a tight 3D structure within the first 4 days of seeding, with high inter-plate reproducibility in terms of size (419 ± 19 μm, RSD = 4.53 %) and following a normal gaussian distribution ($p = 0.9445$, Shapiro-Wilk test) (Supplementary Fig. S2). MCTs were then treated for 72 h with pitavastatin, temozolomide or their combination, at the corresponding 48 h IC_{50} concentration of each drug in monolayer. Medium was partially (50 %) replaced regularly, and the size measured over time up to 17 days, thus introducing a dynamic treatment effect and a longer follow-up period, in comparison to standard 2D models. Pitavastatin (23.81 μM) shows a strong effect in reducing the MCTs size, with consequent blockade of growth, observed from day 10 after seeding ($p < 0.05$) (Fig. 3A). Temozolomide (251 μM) requires a 10-fold higher concentration to achieve a comparable effect. Nonetheless, the kinetic curve also shows an increasing growth trend starting from day 12, which suggests the necessity of maintaining high temozolomide concentrations in order to control the MCTs size or the emergence of drug related resistance mechanisms. The combination therapy shows the most promising anticancer effect, combining the activity of the individual drugs: at the early treatment stage (4–10 days), the curve follows the growth of temozolomide treated MCTs, whereas in the latter phase (10–17 days) it resembles the kinetic pattern of spheroids treated with pitavastatin. MCTs without treatment show a time dependent growth, reaching a mean diameter of 1096 ± 18 μm at day 17.

MCTs shape was evaluated in terms of the circularity of the projected area, taking into consideration their major and minor axis dimensions. A roundness of 1 describes a perfect circle, in opposition to lower values, that reflect an irregular shape. Overall, spheroids show a roundness above 0.85, indicating a regular and round-shaped morphology (Fig. 3B and C). An exception is denoted upon the 72 h treatment with temozolomide, which induced deep structural changes, including ellipsoidal and kidney-like appearances (roundness of 0.72 ± 0.07). At the later treatment stage, specifically, after day 12, MCTs regained their circle-like shape. The microscopic analysis shows that after 72 h of pitavastatin or combination treatment, the MCTs show a less compact and looser shape, which indicates the presence of dead cells, in opposition to the control group, that retains a compact and round morphology.

3.3.2. Invasion studies

Cell invasion was monitored up to 72 h, although the impact of pitavastatin was apparent after 24 h and invasion was inhibited at sub IC_{50} concentrations (Fig. 4A and B). In fact, pitavastatin prevents glioblastoma invasion in a time- and concentration-dependent manner, with concentrations in the low micromolar range (0.25 and 0.5 × IC_{50}, $p < 0.05$). However, temozolomide treated-cells aggressively invade the matrix, indicating that this alkylating drug does not impair the invasion of U87 cells, but may contribute to it. This was observed after 48 and 72 h of treatment with 0.25 × IC_{50} ($p < 0.05$). Interestingly, the combinatory therapy of 0.25 × IC_{50} outperforms the activity of the statin at 48 and 72 h, as the invasion area is significantly reduced ($p < 0.05$). This underlines the synergistic activity of these compounds at this ratio, also verified with their impact in metabolic activity. For the 0.5 × IC_{50}, the invasiveness reflects the performance of the statin alone ($p > 0.05$), which also indicates that pitavastatin overcomes the activity of temozolomide.

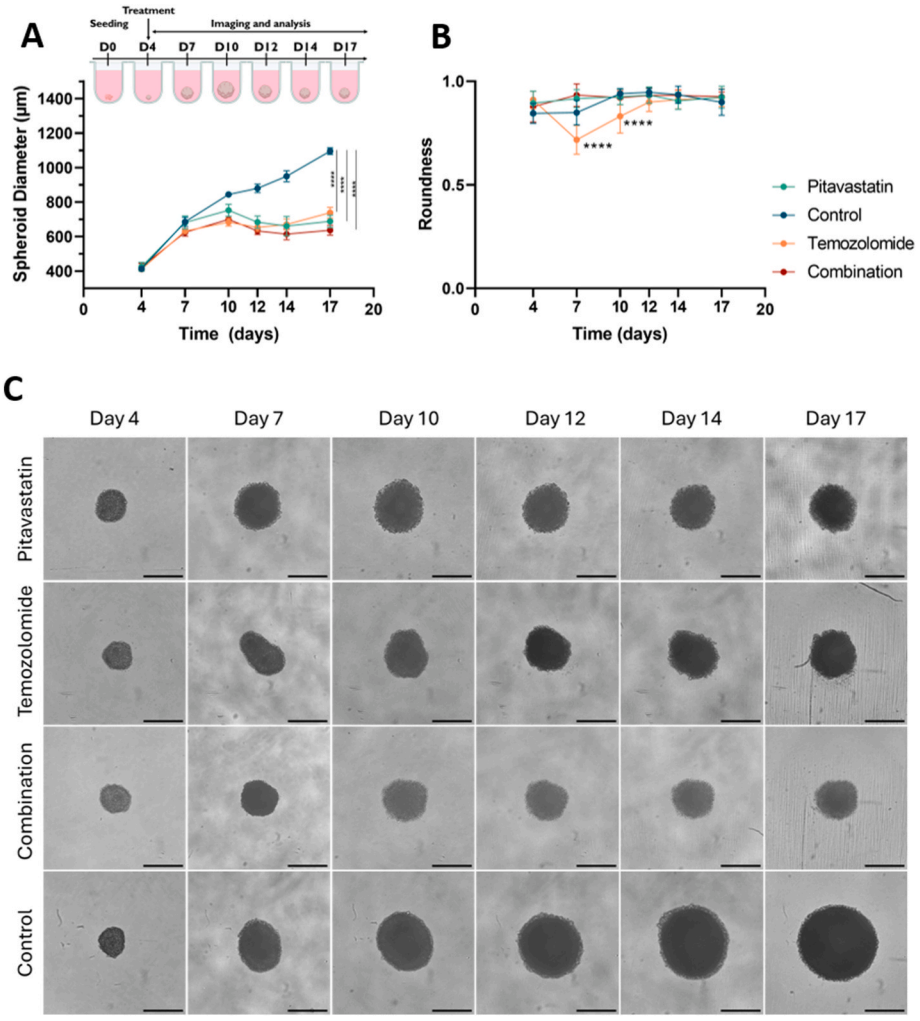

Fig. 3. Growth (**A**) and morphological analysis (**B**) of MCTs treated with the 48 h IC_{50} concentrations of pitavastatin (23.81 μM), temozolomide (251 μM) and their combination (23.81 + 251 μM) over 17 days. Controls were treated with vehicle. Assays were performed in triplicate, in at least three independent experiments, with data being expressed as mean ± SD (one-way ANOVA (α = 0.05) with Dunnett' multiple comparisons (95% CI); ****$p < 0.0001$. Representative photographs (**C**) of U-87 MG MCTs treated with the pitavastatin (23.81 μM), temozolomide (251 μM) and their combination (23.81 + 251 μM) over time. Scale bars represent 500 μm.

3.4. Apoptosis and autophagy mediated cell death

The dual apoptotic and autophagic potential of pitavastatin in inducing cell death was evaluated through the quantification of relevant genes at the transcription level, following a 24 h treatment period. While pitavastatin did not increase the mRNA levels of *BAX*, it led to a significant decrease of *BCL2* and *BCL2L1* mRNAs, thereby disturbing this pathway via BCL-2 and BCL-x_L (Fig. 5). A reduced expression of *BCL2* mRNA was also observed to a lower extent with temozolomide, as well as with the combination of the statin and the standard of care. These results are reflected in the profound disbalance of the *BAX/BCL2* ratio, which shows a 7.2 ± 0.7-fold increase in comparison to untreated cells, *versus* 2.1 ± 0.1 for temozolomide and 2.5 ± 0.5 for the drug combination. The quantification of the tumor suppressor genes *PTEN* and *TP53* was also conducted. A significant increase in *PTEN* mRNA is observed when glioblastoma cells were treated with the drug combination, as well as a slight reduction in *TP53* mRNA, regardless the treatment.

It should be noted that temozolomide also promoted an increase in the mRNA expression of *BECN1* and *LC3B*, which is in agreement with the cytotoxic activity of this drug in glioblastoma (Kanzawa et al., 2004). In what pertains the concurrent administration of the statin and the standard of care, there is also an increase in *BECN1*, *LC3A*, *LC3B* and *ATG5* mRNAs, once again suggesting a cell death mediated by autophagy.

3.5. Proteomics

3.5.1. Proteomic landscape of pitavastatin treated cells

The impact of pitavastatin on the proteome of U-87 MG cells was evaluated following a 24 h treatment period through LC-MS/MS. Out of 4220 proteins, 1936 were identified in all samples and were thus considered for the analyses. These represent a wide variety of proteins with different expression patterns amongst the samples (Fig. 6A). The Row-wise correlation between each replicate was estimated to ensure data's reproducibility (Fig. 6B). As such, there is a direct correlation between each two samples, as indicated by the Pearson coefficients ($R \geq 0.989$). As anticipated, the correlation between each combination of control *vs*. pitavastatin is slightly lower ($0.984 \leq R \leq 0.989$). The higher dispersion of the data suggests, *a priori*, the presence of up and down-regulated proteins. Principal component analysis shows a clear separation between both groups on PC1, representing 41.2 % of the variance and supporting the drug treatment as the driving force of protein expression deregulation (Fig. 6C).

In order to gain insights on the molecular basis of the treatment, a volcano plot with a two-sided *t*-test (FDR <0.05, S0 = 0.1) comparing treated with nontreated cells was drawn, thus unveiling the proteins with different expression patterns (Fig. 7A). Out of the 254 proteins identified, 166 are downregulated, whereas the remaining 88 are upregulated. There are also 51 proteins that were only identified in the

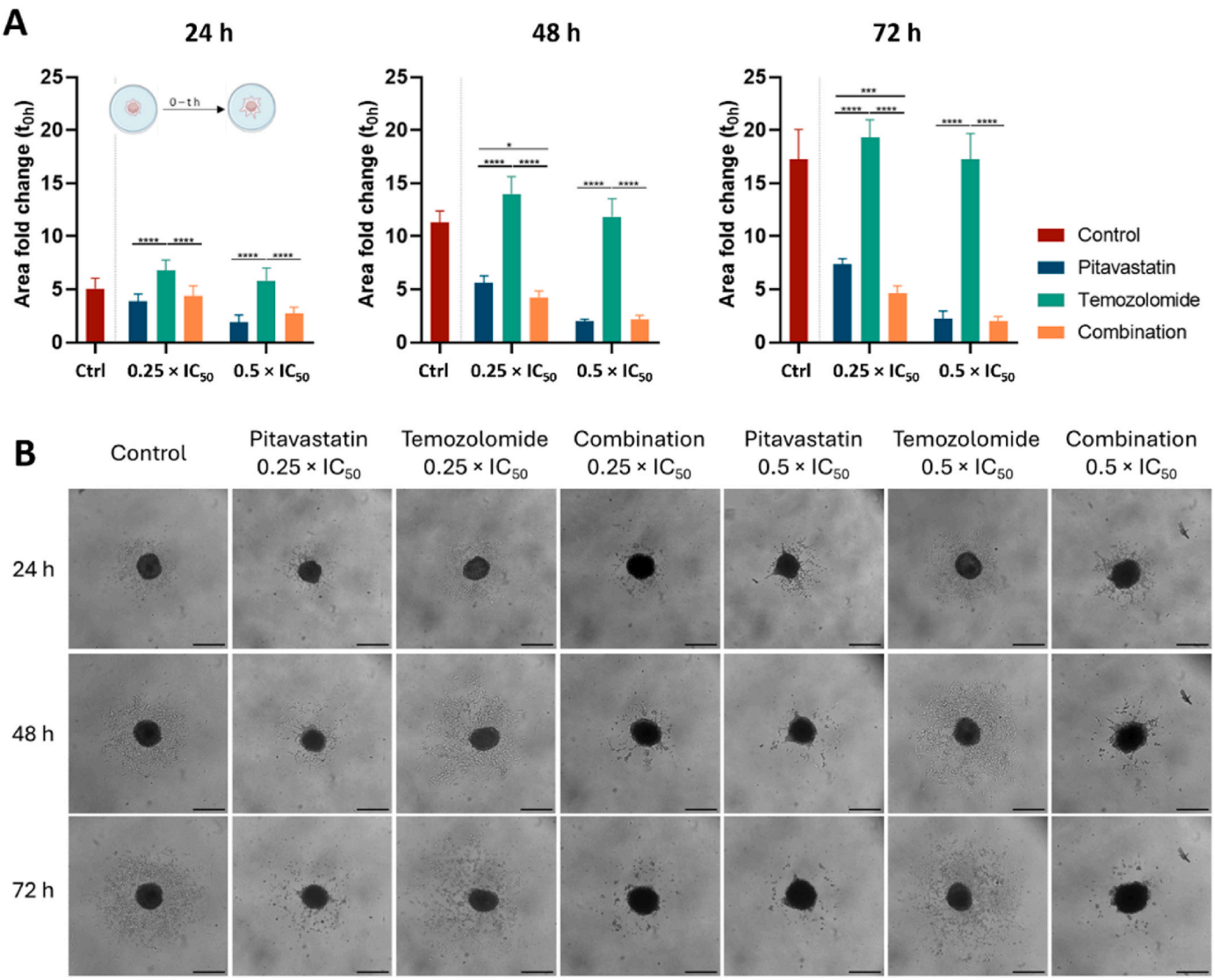

Fig. 4. Invasion (**A**) of U-87 MG MCTs treated with fixed-dose ratios (0.25 and 0.5 × IC_{50}, at 48 h) of pitavastatin, temozolomide and their combination for 24, 48 and 72 h. Assays were performed in triplicate, in at least three independent experiments, with data being expressed as mean ± SD (one-way ANOVA ($\alpha = 0.05$) with Tukey's multiple comparisons (95% CI)); *$p < 0.05$, ***$p < 0.001$, ****$p < 0.0001$. Representative photographs (**B**) of day 4 U–87 MG MCTs placed on collagen-coated plates and treated with different concentrations of pitavastatin, temozolomide and their combination. Controls were treated with vehicle. Images were captured daily, up to 72 h, using an inverted microscope. Scale bars represent 500 μm.

three replicates of the control or pitavastatin group (31 up and 20 downregulated).

The top up and downregulated proteins are presented in Table 1. Overall, pitavastatin downregulates several oncogenic proteins, including HTRA1, SERPINE1, KPNA2, WNT5A, VCAN, ALDH3B1, EPHA2, TYMS, GNAI3 and TGFBI. Hierarchical clustering analysis clearly depicts differentially regulated proteins in response to pitavastatin treatment and determines the direction of protein expression (Fig. 7B).

A Molecular Complex Detection (MCODE) clustering analysis was conducted to identify dense regions and molecular complexes of the protein-protein interaction network involved in glioblastoma cells treated with pitavastatin, while avoiding false positives from high-throughput interaction techniques (Palukuri et al., 2023). A total of five protein clusters were identified (Fig. 8). The first cluster reflects the biological processes that occur in the nucleus of the cells, in particular, those related to the chromosomal region. Accordingly, pitavastatin leads to an impairment in the DNA metabolic processes, in terms of DNA replication, conformation changes and unwinding, as there is a significant downregulation of several DNA supporting enzymes. The second cluster expresses the influence in the ribonucleoprotein complex, with modifications in mRNA splicing and miRNA processing. The third cluster is related to the regulation of the extracellular space, as it describes the role of this statin in the homeostasis of the ECM and in integrin-cell surface interactions. The fourth and fifth clusters depict the disturbance of the pentose phosphate pathway, nucleotide biosynthesis, amino acid and carbon metabolism, nuclear pore complex disassembly and MAPK pathway.

4. Discussion

Glioblastoma cells were treated with different concentrations of pitavastatin and showed a distinct behavior in what pertains cell proliferation and metabolic activity. Although in the low micromolar range, the differences in IC_{50} magnitudes suggest that, despite disturbing essential metabolic pathways, the genetic background of tumor cells strongly dictates drug response. For example, while pitavastatin may be internalized by passive diffusion, the different expression of organic

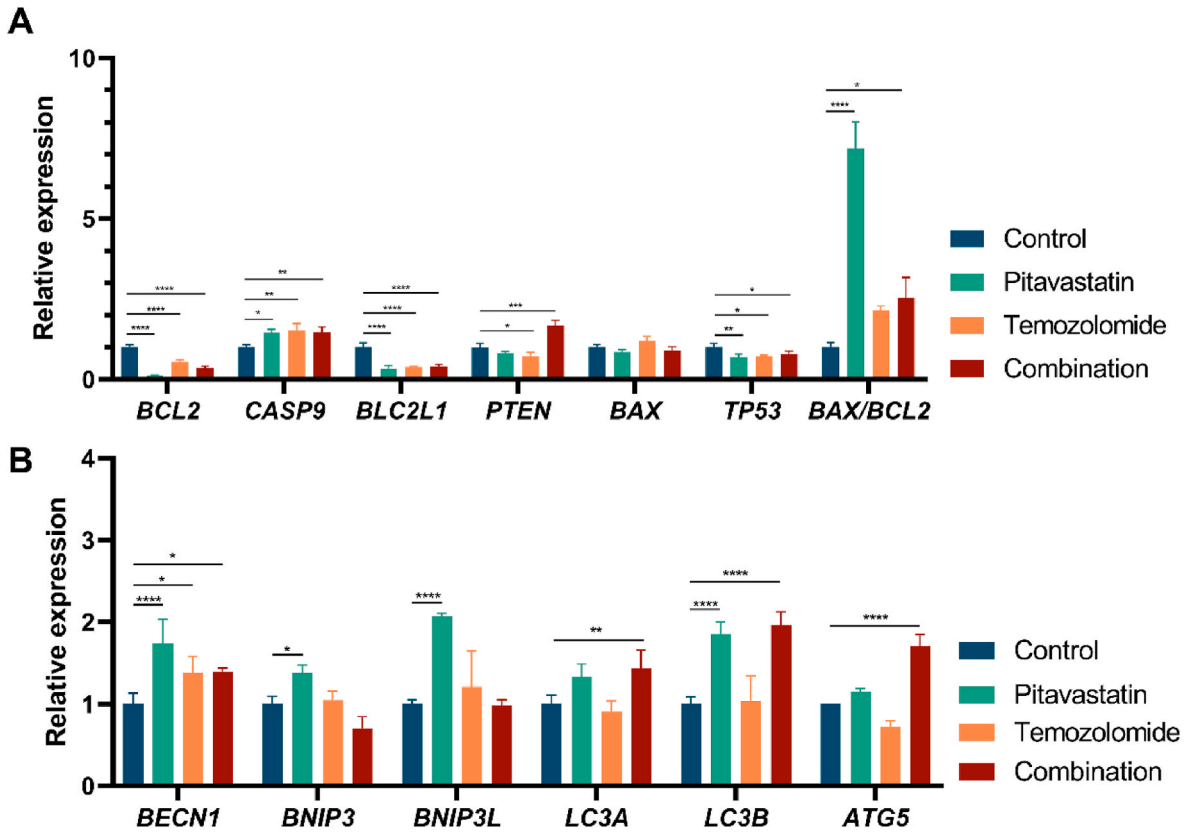

Fig. 5. Quantification of mRNA expression of (**A**) apoptosis and (**B**) autophagy related genes in U-87 MG cells treated with the 48 h 0.25 × IC_{50} of pitavastatin, temozolomide and their combination for 24 h. The assays were performed in at least three independent experiments with data being expressed as mean ± SD (one-way ANOVA ($\alpha = 0.05$) with Dunnett's multiple comparisons (95% CI); *$p < 0.05$, **$p < 0.01$, ***$p < 0.001$, ****$p < 0.0001$ vs control.

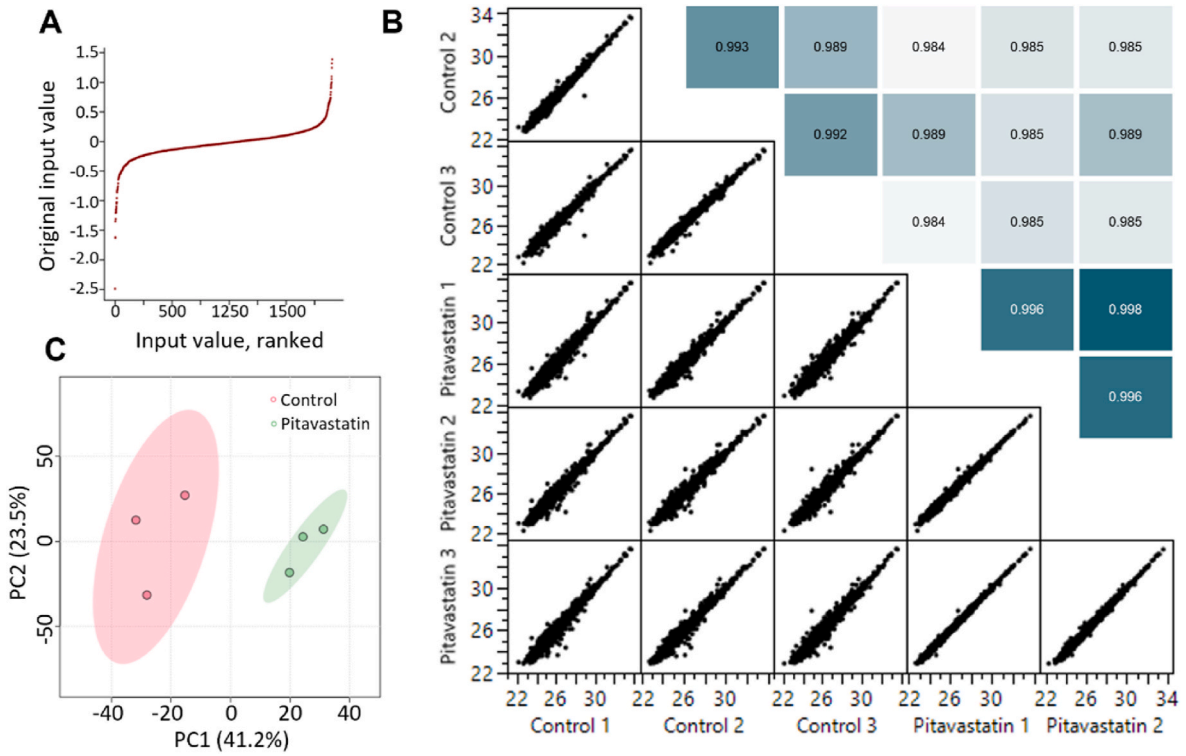

Fig. 6. Proteomic analysis of pitavastatin-treated cells for 24 h. **A**) Expression overview of the identified proteins. **B**) Row-wise correlation analysis showing a positive linear relationship between samples. **C**) Principal component analysis demonstrates a clear distinction between the proteome of pitavastatin-treated cells and control.

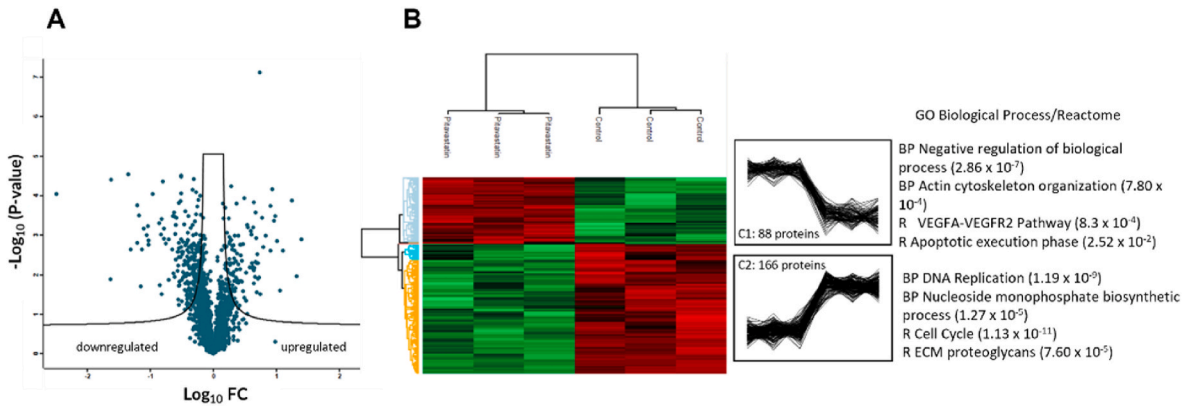

Fig. 7. **A**) Volcano scatter plot of pitavastatin-treated glioblastoma cells *vs.* control. The red and blue dots indicate proteins significantly ($q < 0.05$) upregulated and downregulated respectively (two-sided *t*-test, FDR <0.05, S0 = 0.1). **B**) Hierarchical clustering analysis of normalized protein concentrations. Each row represents a distinct protein, and each column represents a biological independent replicate. Red and green represent positive and negative z scores, respectively. FDR of Biological Processes/Reactome are presented in parentheses.

Table 1
Top down and upregulated proteins in U-87 MG cells treated with pitavastatin.

Top downregulated				
-LOG(P-value)	Difference	Protein	Tumour Expression in patients	Activity in glioblastoma
4.040	−2.489	HTRA1	↑[a]	HTRA1 knockdown reduces cell viability, EMT, migration and invasion by mediating the HDAC6/Ac-α-tubulin pathway (Zhao et al., 2024).
4.415	−1.619	SERPINE1	↑[a]	SERPINE 1 knockdown reduces growth, migration and cell adhesion in a 3D tumour model. It also reduces WNT5A expression (Seker et al., 2019).
4.543	−1.349	KPNA2	↑[a]	KPNA2 knockdown decreases deoxyglucose uptake, lactate production and oxidative phosphorylation, via c-myc. Tumour proliferation and invasiveness were concomitantly downregulated (Li et al., 2018).
2.645	−1.310	WNT5A	↑[a]	WNT5A is highly expressed in mesenchymal glioblastoma. In vivo inhibition of Wnt5a activity impairs brain invasion and tumour growth (Binda et al., 2017).
2.810	−1.208	VCAN	↑[a]	VCAN overexpression, a major component of the ECM, is involved in cell adhesion, motility and migration via TGF-β2 (Arslan et al., 2007).
3.759	−1.206	ALDH3B1	↑[a]	ALDH3B1 silencing decreases cell proliferation, migration, colony formation and EMT (Wang et al., 2022b).
3.508	−1.178	EPHA2	↑[a]	EPHA2 knockdown decreases cell viability and invasiveness, and is associated to classical and mesenchymal subtypes (Gai et al., 2022).
2.638	−1.131	TFPI2	= (↑ trend)	TFPI2 is associated to stem cell self-renewal, tumour growth, microglia infiltration and immunosuppressive polarization (Pang et al., 2023).
3.170	−1.098	RPL27A	↑[a]	Unknown. In triple-negative breast cancer, targeting RPL27A reduces cell migration and invasion (Zhao et al., 2021).
3.011	−1.053	TYMS	↑[a]	TYMS knockdown reduces cell proliferation, increases apoptosis and sensitizes cells to temozolomide (Zhao et al., 2019).
3.232	−1.037	GNAI3	↑[a]	Increased expression is associated to a poorer overall prognosis and disease-free survival (Raza et al., 2023)
2.878	−1.025	CNN2	↑[a]	Unknown. In hepatic and gastric cancer, CNN2 downregulation inhibits cell proliferation, migration and invasion (Hu et al., 2017; Kang et al., 2018)
2.767	−1.023	TGFBI	↑[a]	ECM protein involved in cell proliferation, migration, invasion and apoptosis (Guo et al., 2018). Upstream regulator of SERPINE 1 (Seker et al., 2019).
Top upregulated				
-LOG(P-value)	Difference	Protein	Tumour Expression in patients	Activity in glioblastoma
2.906	1.391	ACTN4	= (↑ trend)	Isoform of non-muscular α-actinin and actin-bundling protein with a role in cancer invasion by increasing cellular motility (Fukushima et al., 2014).
1.97	1.321	SNRNP70	= (↓ trend)	Constitutive protein of the spliceosome, is upregulated in long-term survivors (Lié et al., 2022).
3.886	1.246	HSPB1	↑[a]	HSPB1 expression is associated to a reduced overall survival and higher malignancy, regulated upstream by EGFR (Gimenez et al., 2015).
2.611	1.098	CORO1C	↑[a]	Key player in actin rearrangement and cofilin dynamics, with impact on the migration of tumour cells (Mustafov et al., 2023).
1.606	1.053	MT1E	= (no trend)	MT1E promotes cell migration and invasion through MMP-9 inactivation (Ryu et al., 2012)
2.863	1.004	PLTP	↑[a]	PLTP knockdown decreases cell growth, migration and EMT (Dong et al., 2017).

[a] $p < 0.05$ (vs healthy subjects, TCGA/GTEx data)(Tang et al., 2019).

anion transporting polypeptide (OATP) receptors in glioblastoma may modulate the internalization extension of the statin (Cooper et al., 2022; Fujino et al., 2004). The metabolic activity results are in accordance with the work of Jiang P. et al., who obtained similar IC_{50} values following 48 and 72 h of treatment (Jiang et al., 2014a). Accordingly, pitavastatin has shown to be the most promising drug in a pool of seven statins, with a strong *in vitro* activity and a good correlation with *in vivo* results. Pitavastatin outperformed both cerivastatin (IC_{50} = 1.37 μM, 48 h) and fluvastatin (IC_{50} = 19.32 μM, 48 h) in a U-87 MG heterotopic glioblastoma mice model, in which cerivastatin led to a less pronounced tumor reduction and fluvastatin did not exert any effect, in spite of the higher *in vitro* activity. These dissimilarities between the *in vitro/in vivo*

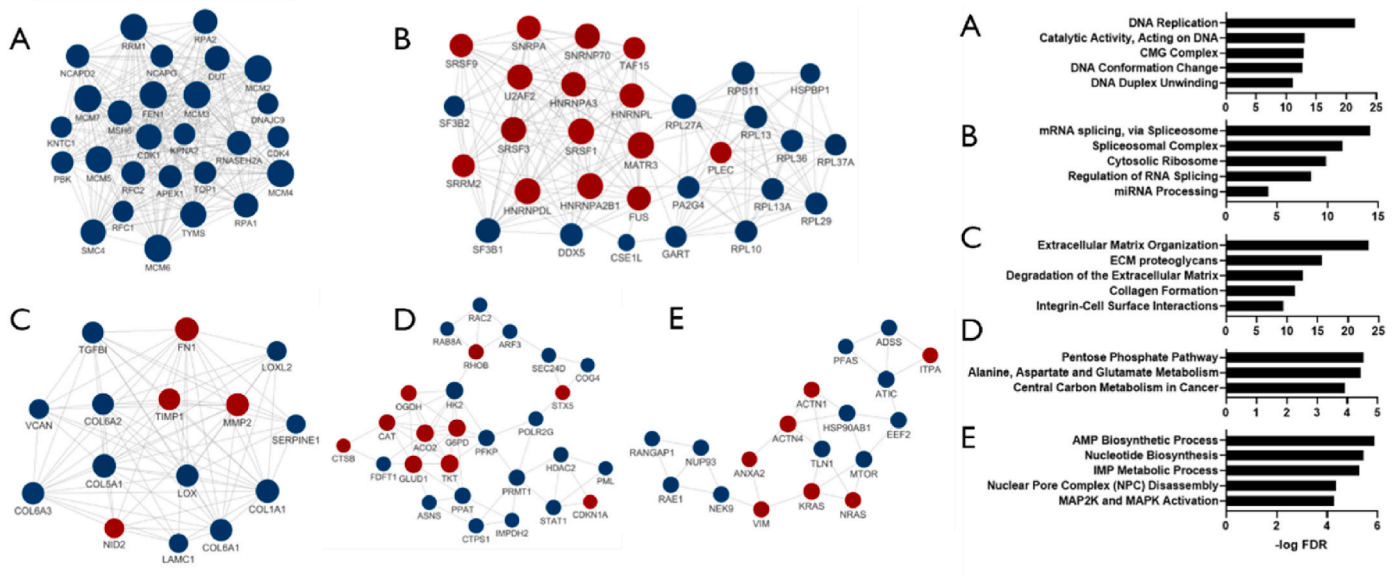

Fig. 8. Protein-protein network clusters of deregulated proteins, identified by Molecular Complex Detection. Red and blue dots indicate proteins significantly ($q < 0.05$) upregulated and downregulated, respectively.

activity may be explained by the intrinsic properties of the drugs, with differences in pharmacokinetics (rate and extent of absorption, distribution, metabolism and excretion), lipophilicity and the blood-brain-barrier permeability.

The combined activity of pitavastatin and the standard of care, temozolomide, was inspected in U-87 MG cell monolayers, in which the statin showed the highest IC_{50}. Interestingly, this treatment results in different pharmacological effects, depending on the combination pair: at the lowest concentration, there is a synergistic activity that contrasts to the competitive/antagonistic interaction at the highest concentration under study. However, this latter interaction arises when using temozolomide and pitavastatin concentrations that are not achieved in clinical practice, but are essential for understanding their full pharmacodynamic profile. In fact, brain interstitial and cerebral spinal fluid temozolomide concentrations, measured by microdialysis and liquid chromatography converge towards the $0.25 \times IC_{50}$ concentration (Büsker et al., 2022; Portnow et al., 2009). Similarly, the $0.25 \times IC_{50}$ pitavastatin concentration approaches the plasma concentration of healthy volunteers after a single oral administration of 3 mg (Lv et al., 2007). This not only underlines the high resistance of glioblastoma to this alkylating agent, but also corroborates the promising synergism between these drugs in a relevant clinical context.

Although 2D models are widely used to evaluate drug response, the transposition to 3D models provides a biologically relevant framework that contributes to the generation of robust data. MCTs are 3D structures that may be formed by self-assembling when cultured under controlled scaffold-free conditions. These cellular aggregates, if presenting a diameter higher than 500 μm, are characterized by hypoxic regions and necrotic centers, closely resembling pivotal features of tumors *in vivo* (Han et al., 2021). In addition, they present marked molecular differences when compared to standard 2D cultures, including a reduced nucleotide, purine, amino acid and glutathione metabolism, an increased *de novo* lipid biosynthesis and a transition from aerobic (TCA cycle) to anaerobic energy synthesis (glycolysis) (Wen et al., 2024). The impact of pitavastatin, temozolomide and their combination on MCTs was evaluated, with the combination treatment providing the most promising results. One of the hallmarks of glioblastoma is the profound infiltration of the tumors to the surrounding tissue. Although not metastasizing frequently, glioblastoma cells are able to cross local barriers through ECM and cytoskeleton remodeling, both individually and collectively (Kim et al., 2021; Vollmann-Zwerenz et al., 2020). 3D invasion was evaluated in a collagen I-coated matrix, a semi-solid gel like support that provides an MMP-dependent barrier into which cells extend invadopodia (Sodek et al., 2008). These contribute to cell movement and matrix degradation due to localized proteolysis. Similarly to the previous results, low micromolar concentrations of the statin strongly impair cell motility and invasion, contrasting to the activity of temozolomide. In fact, a short-term treatment with 25 μM of temozolomide was reported to increase the motility and displacement of glioblastoma cells, with an enriched sub population of highly motile cells after 72 h (Kochanowski et al., 2021).

The evaluation of the apoptotic and autophagic potential in inducing cell death was evaluated at the transcription level. The intrinsic apoptotic pathway derives from the mitochondria membrane permeabilization with consequent activation of caspases 9 and 3/7 and several hydrolases that ultimately lead to nuclear condensation and fragmentation, along with blebbing of the plasma membrane and formation of apoptotic bodies (Das et al., 2021). This cascade of events is maintained by a delicate balance between the pro- and the antiapoptotic proteins BAX and BCL-2/BCL2-XL, respectively. In fact, the decrease of *BCL2* and *BCL2L1* mRNAs with the disbalance of the *BAX/BCL2* ratio and the upregulation of *CASP9* mRNA levels by both drugs, alone or in combination, may suggest that cell death occurs by apoptosis via the caspase-dependent mitochondrial pathway. Within the context of gliomas, pitavastatin has also been shown to strongly reduce *NFKB1* and *BIRC1* mRNA levels, both involved in apoptosis inhibition through the neutralization of active caspases (Chauhan et al., 2021).

Even though autophagy is commonly a cytoprotective response that degrades and eliminates misfolded proteins and damaged organelles, it may also trigger proapoptotic events that further lead to cell death (Marino et al., 2014). For instance, pitavastatin treated cells show an increased expression of *BNIP3*, a known regulator that mediates the expression of *BECN1* via *BCL2*. In fact, this overexpression is associated with the downregulation of BCL2, thereby acting as a bridge between autophagy and apoptosis (Marquez and Xu, 2012). The overexpression of different markers that affect different stages of autophagy, including *BECN1*, *BNIP3* and *BNIP3L* and *LC3B,* supports the potential of pitavastatin in promoting the death of glioblastoma cells through this pathway. In addition, pitavastatin-treated glioma cells have shown extensive cell vacuolization, as well an enhanced LC3-I to LC3-II conversion, two key features of autophagy (Jiang et al., 2014b).

The proteome landscape of pitavastatin treated glioblastoma cells

was also assessed. Overall, pitavastatin downregulates several oncogenic proteins, including HTRA1, SERPINE1, KPNA2, WNT5A, VCAN, ALDH3B1, EPHA2, TYMS, GNAI3 and TGFBI. These are overexpressed in glioblastoma patients and modulate different processes, including cell proliferation and tumor growth, migration, invasion, epithelial to mesenchymal transition (EMT) and extracellular matrix (ECM) turnover (Arslan et al., 2007; Binda et al., 2017; Gai et al., 2022; Guo et al., 2018; Li et al., 2018; Raza et al., 2023; Seker et al., 2019; Wang et al., 2022b; Zhao et al., 2019, 2024).

Enrichment analysis identified two clusters and shows that the anticancer treatment is associated with intra and extracellular processes: pitavastatin impairs DNA replication and nucleoside biosynthesis, induces structural actin mediated deformations, apoptosis, and modulates angiogenesis as well as the composition of the extracellular matrix.

The disorganization of the actin cytoskeleton fibers with cell rounding and loss of morphological structure was also observed by optical microscopy upon pitavastatin treatment. This is a known trigger for apoptosis and has been described in literature (Desouza et al., 2012; Rodríguez-Expósito et al., 2022). The proangiogenic activity of statins via VEGF release is also reported, and is known to be dependent on the statin concentration: statins are proangiogenic at low doses, but angiostatic at high doses (Weis et al., 2002). The activation of the constitutive TGFB pathway is the major player in VEGF release by glioblastoma cells and is associated to a poor clinical prognosis (Seystahl et al., 2015). Pitavastatin treated cells show a 2-fold reduction in TGFBI levels, which is consistent with the inhibitory activity of the TGFBI/VEGF axis by simvastatin and atorvastatin (Bayat et al., 2018; Xiao et al., 2019). In addition, they have shown a promising activity in inducing apoptosis, autophagy and sensitizing tumor cells to chemotherapy (Sahebkar et al., 2021; Zahedipour et al., 2022). This is in agreement with the data previously obtained from the combination studies with temozolomide and transcriptional quantification of genes with apoptotic and autophagic function.

According to the results, pitavastatin also leads to modifications in the extracellular space. The ECM is an acellular component that regulates tumor development through modifications in macromolecule component, degradation enzymes and stiffness, and is controlled by the different cells in the tumor microenvironment. It also acts as a rock-solid physical barrier that hinders a successful anticancer treatment (Yuan et al., 2023). Pitavastatin reduces the expression (2–3 fold change) of different proteins associated to the ECM turnover, with a highlight for VCAN (chondroitin sulfate proteoglycan, a major component of the ECM (Arslan et al., 2007)), SERPINE1 (a serine protease inhibitor that reduces ECM proteolysis and cell detachment (Seker et al., 2019)) and TGFBI. In parallel, this statin activity may also be related with EMT through the downregulation of different markers associated to the transcriptional mesenchymal subtype of glioblastoma, a more aggressive phenotype with higher rates of proliferation, angiogenesis, invasiveness and resistance (Steponaitis and Tamasauskas, 2021). These include HTRA1, SERPINE1, WNT5A, ALDH3B1 and EPHA2. The EMT inhibition by statins is also supported by their intrinsic activity in the mevalonate cascade, that decreases the biosynthesis of isoprenoids, affecting cell stemness, polarity, motility and adhesion (Gruenbacher and Thurnher, 2018; Sahebkar et al., 2021). These results are in agreement with the reduced invasion of MCTs derived cells previously observed (Section 3.3.2). Paradoxically, pitavastatin also upregulates proteins with a derogatory activity in glioblastoma, specifically, ACTN4, HSPB1, CORO1C and MT1E. However, it is postulated that this increase in protein expression is not accompanied by an oncogenic outcome, as supported by the remaining data.

The metabolic reprogramming that sustains tumor development and progression is associated with the Warburg effect, a shift from the tricarboxylic acid (TCA) cycle and oxidative phosphorylation to glycolysis and glutaminolysis, with glucose consumption and lactate and glutamate production (Liberti and Locasale, 2016). This allows tumor cells to maintain the production of citrate, acetyl-CoA and other metabolites, thereby fueling the mevalonate pathway (Pereira et al., 2022). The biosynthesis of cholesterol and isoprenoids, in parallel with the prenylation (farnesylation and geranylgeranylation) of different proteins with GTPase activity (such as Rho, Ras, Rheb), disturbs the Hippo pathway through the activation of YAP and TAZ and contributes to the malignancy and stemness of glioblastoma cells (Koo and Guan, 2018; Wang et al., 2017b). These oncogenes, along with mutant p53, upregulate SREBP-2 and induce the transcription of genes related to the mevalonate pathway through a positive feedback loop (Parrales et al., 2018). Geranylgeranyl depletion is also a trigger for autophagy induction, via AMPK (Gorabi et al., 2021). In parallel, Rho GTPase proteins also promote GLUT1 translocation, increasing glucose uptake and glycolysis and regulate the actin cytoskeleton of the cell. Consequently, this protein family assumes a pivotal role in cell division, endocytosis, cell migration and invasion (Haga and Ridley, 2016; Wang et al., 2022a). The anticancer activity of pitavastatin in glioblastoma is intimately linked to the inhibition of the mevalonate pathway and the aforementioned processes, leading to an imbalanced cell signaling. Our results show that, as a result of HMG Co-A reductase inhibition, there is a decrease in *BCL2* and *BCL2L1* mRNA, which trigger apoptosis. This programmed cell death is reversed by mevalonate and geranylgeranyl pyrophosphate, the latter being a key player in protein geranylgeranylation. Interestingly, the reintroduction of cholesterol, geranylpyrophosphate, isopentenyl pyrophosphate or farnesyl pyrophosphate, mediator of farnesylation, does not overcome pitavastatin mediated cell death (Jiang et al., 2014a). In parallel, the upregulation of *BECN1*, *BNIP3* and *BNIP3L* mRNA supports the involvement of autophagy and mitophagy, through vesicle formation, which is later accompanied by the fusion of autophagosomes with lysosomes via LC3A/B and LC3-I to 3-II conversion. As a result, glioblastoma cells treated with pitavastatin undergo extensive cell death (Fig. 9). This statin has a pro apoptotic effect, via FOXO3a, caspase 3, cleaved PARP and cytochrome *c* release in other types of cancer (Lee et al., 2020; You et al., 2016).

5. Conclusions

The limited effectiveness of chemotherapy in glioblastoma, underlined by the reduced therapeutic arsenal, is a major cause that contributes to the reduced overall survival commonly observed in these patients. Subsequently, there is an active demand for novel approaches that converge towards a successful treatment with a measurable impact on overall and disease-free survival. Pitavastatin has emerged as a drug candidate via repositioning, as it shows promising preclinical results in the treatment of different types of cancer. This work deepens the limited knowledge of the potential of this statin in cancer, through the use of different 2D and 3D glioblastoma models.

Pitavastatin shows a strong antiproliferative activity over various glioma and glioblastoma cell lines (A-172, H4, U118-MG, U-87 MG, U373 MG), inducing a significant cell death, in what pertains IC_{50}, at concentrations below 25 μM. Interestingly, not only is pitavastatin 10-1000 times-fold more effective in reducing metabolic activity that temozolomide, but it also revealed a synergistic activity with the clinical standard of care, thereby acting as chemo-sensitizing and reducing the required local concentration that results in cell death. Pitavastatin was additionally evaluated in a 3D glioblastoma model, a biologically relevant framework that contributes to the generation of robust data. MCTs treated with a low micromolar concentration of pitavastatin (ca. 25 μM) show a strong reduction in size with consequent growth impairment from day 10 to day 17. In addition, the combination of pitavastatin with temozolomide leads to the smallest MCTs, with a prominent growth delay. Further studies show an extensive prevention of glioblastoma invasion in a time and concentration dependent manner, in contrast to temozolomide. Yet, an additional impact on cell invasion was observed when MCTs were treated with both drugs at a sub IC_{50} concentration ($0.25 \times IC_{50}$) at 48 and 72 h. Together with the combination studies and MCTs kinetics evaluation, this analysis also supports the potential

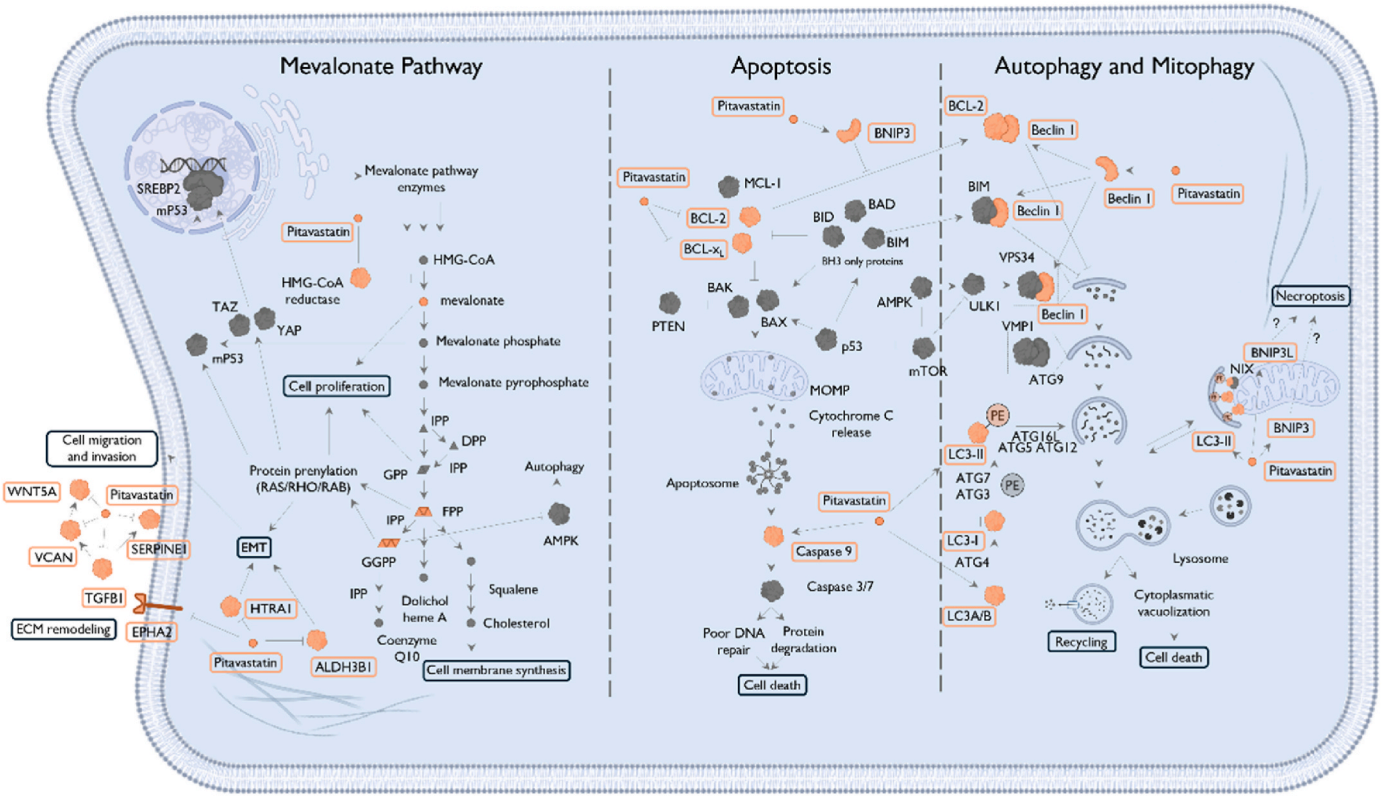

Fig. 9. Proposed anticancer mechanism of action of pitavastatin in glioblastoma. Pitavastatin induces cell death of glioblastoma cells via inhibition of the mevalonate pathway, impairing protein prenylation and consequent cell signaling. Relevant genes affected by pitavastatin are represented in orange.

adjuvant benefits of this statin in the treatment of glioblastoma.

Bearing in mind that the mechanism of action of pitavastatin in this cancer is poorly described in literature, qRT-PCR and proteomics were applied to investigate different targets that disrupt the molecular cascades that drive tumor progression, migration and invasion. The results suggest the modulation of cell death via apoptosis (*BAX/BCL2, CASP9*) and autophagy/mitophagy (*BECN1, BNIP3*, *BNIP3L* and *LC3B*), as well as the downregulation of several proteins with a role in epithelial to mesenchymal transition (HTRA1, SERPINE1, WNT5A, ALDH3B1 and EPHA2) and remodeling of the extracellular matrix (VCAN, SERPINE1 and TGFBI).

Overall, the results of this study highlight the promising potential of pitavastatin as a therapeutic strategy for glioblastoma, laying the foundation for further investigations on the potential combinatory clinical treatment with the current standard of care.

CRediT authorship contribution statement

João Basso: Writing – original draft, Software, Methodology, Investigation, Formal analysis, Conceptualization. **Ana Miguel Matos:** Writing – review & editing, Methodology. **Saeid Ghavami:** Writing – review & editing. **Ana Fortuna:** Writing – review & editing, Supervision. **Rui Vitorino:** Writing – review & editing, Supervision, Software, Formal analysis, Conceptualization. **Carla Vitorino:** Writing – review & editing, Supervision, Funding acquisition, Formal analysis, Conceptualization.

Ethics approval and consent to participate

There are no ethical issues to declare.

Consent for publication

The authors consent for publication.

Availability of data and materials

The data presented to reproduce the findings in this study are included in the article and supplementary material. The raw data are available on reasonable request from the corresponding author (C.V.).

Declaration of competing interest

The authors declare that there is no financial/personal interest or belief that could affect the manuscript objectivity.

Funding and Acknowledgements

This research was funded by the Portuguese Foundation for Science and Technology (FCT), European Union, QREN, FEDER, COMPETE and PIDDAC for funding the iBiMED (UIDB/04501/2020, POCI-01-0145-FEDER-007628), Unidade de Investigação Cardiovascular (UID/IC/00051/2019), and the Coimbra Chemistry Center, CQC (UID/QUI/00313/2020, doi:10.54499/UIDB/00313/2020). João Basso also acknowledges FCT for the PhD research grants (SFRH/BD/149138/2019 and COVID/BD/153479/2023).

Appendix A. Supplementary data

Supplementary data to this article can be found online at https://doi.org/10.1016/j.ejphar.2024.177087.

Data availability

Data will be made available on request.

References

Afshari, A.R., Mollazadeh, H., Henney, N.C., Jamialahmad, T., Sahebkar, A., 2021. Effects of statins on brain tumors: a review. Semin. Cancer Biol. 116–133. Elsevier.

Alrosan, A.Z., Heilat, G.B., Al Subeh, Z.Y., Alrosan, K., Alrousan, A.F., Abu-Safieh, A.K., Alabdallat, N.S., 2023. The effects of statin therapy on brain tumors, particularly glioma: a review. Anti Cancer Drugs 34, 985–994.

Arslan, F., Bosserhoff, A., Nickl-Jockschat, T., Doerfelt, A., Bogdahn, U., Hau, P., 2007. The role of versican isoforms V0/V1 in glioma migration mediated by transforming growth factor-β2. Br. J. Cancer 96, 1560–1568.

Basso, J., Miranda, A., Sousa, J., Pais, A., Vitorino, C., 2018. Repurposing drugs for glioblastoma: from bench to bedside. Cancer Lett. 428, 173–183.

Basso, J., Sereno, J., Fortuna, A., Castelo-Branco, M., Vitorino, C., 2021. Establishing orthotopic xenograft glioblastoma models for use in preclinical development. Nanotherapy for Brain Tumor Drug Delivery 281–296.

Bayat, N., Izadpanah, R., Ebrahimi-Barough, S., Javidan, A.N., Ai, A., Ardakan, M.M.M., Saberi, H., Ai, J., 2018. The anti-angiogenic effect of atorvastatin in glioblastoma spheroids tumor cultured in fibrin gel: in 3D in vitro model. Asian Pac. J. Cancer Prev. APJCP: Asian Pac. J. Cancer Prev. APJCP 19, 2553.

Binda, E., Visioli, A., Giani, F., Trivieri, N., Palumbo, O., Restelli, S., Dezi, F., Mazza, T., Fusilli, C., Legnani, F., 2017. Wnt5a drives an invasive phenotype in human glioblastoma stem-like cells. Cancer Res. 77, 996–1007.

Büsker, S., Jäger, W., Poschner, S., Mayr, L., Al Jalali, V., Gojo, J., Azizi, A.A., Ullah, S., Bilal, M., El Tabei, L., 2022. Pharmacokinetics of metronomic temozolomide in cerebrospinal fluid of children with malignant central nervous system tumors. Cancer Chemother. Pharmacol. 89, 617–627.

Chauhan, P.S., Kumarasamy, M., Carcaboso, A.M., Sosnik, A., Danino, D., 2021. Multifunctional silica-coated mixed polymeric micelles for integrin-targeted therapy of pediatric patient-derived glioblastoma. Mater. Sci. Eng. C 128, 112261.

Chou, T.-C., 2010. Drug combination studies and their synergy quantification using the Chou-Talalay methodsynergy quantification method. Cancer Res. 70, 440–446.

Cooper, E., Woolf, Z., Swanson, M.E., Correia, J., Schweder, P., Mee, E., Heppner, P., Turner, C., Faull, R.L., Scotter, E.L., 2022. Single-cell image analysis reveals over-expression of organic anion transporting polypeptides (OATPs) in human glioblastoma tissue. Neuro-Oncology Advances 4, vdac166.

Das, S., Shukla, N., Singh, S.S., Kushwaha, S., Shrivastava, R., 2021. Mechanism of interaction between autophagy and apoptosis in cancer. Apoptosis 1–22.

Dastghaib, S., Shojaei, S., Mostafavi-Pour, Z., Sharma, P., Patterson, J.B., Samali, A., Mokarram, P., Ghavami, S., 2020. Simvastatin induces unfolded protein response and enhances temozolomide-induced cell death in glioblastoma cells. Cells 9, 2339.

Desouza, M., Gunning, P.W., Stehn, J.R., 2012. The actin cytoskeleton as a sensor and mediator of apoptosis. BioArchitecture 2, 75–87.

Dong, W., Gong, H., Zhang, G., Vuletic, S., Albers, J., Zhang, J., Liang, H., Sui, Y., Zheng, J., 2017. Lipoprotein lipase and phospholipid transfer protein overexpression in human glioma cells and their effect on cell growth, apoptosis, and migration. Acta Biochim. Biophys. Sin. 49, 62–73.

Fu, M., Zhou, Z., Huang, X., Chen, Z., Zhang, L., Zhang, J., Hua, W., Mao, Y., 2023. Use of Bevacizumab in recurrent glioblastoma: a scoping review and evidence map. BMC Cancer 23, 544.

Fujino, H., Nakai, D., Nakagomi, R., Saito, M., Tokui, T., Kojima, J., 2004. Metabolic stability and uptake by human hepatocytes of pitavastatin, a new inhibitor of HMG-CoA reductase. Arzneimittelforschung 54, 382–388.

Fukushima, S., Yoshida, A., Honda, K., Maeshima, A.M., Narita, Y., Yamada, T., Shibui, S., Tsuda, H., 2014. Immunohistochemical actinin-4 expression in infiltrating gliomas: association with WHO grade and differentiation. Brain Tumor Pathol. 31, 11–16.

Gai, Q.-J., Fu, Z., He, J., Mao, M., Yao, X.-X., Qin, Y., Lan, X., Zhang, L., Miao, J.-Y., Wang, Y.-X., 2022. EPHA2 mediates PDGFA activity and functions together with PDGFRA as prognostic marker and therapeutic target in glioblastoma. Signal Transduct. Targeted Ther. 7, 33.

Gimenez, M., Marie, S.K.N., Oba-Shinjo, S., Uno, M., Izumi, C., Oliveira, J.B., Rosa, J.C., 2015. Quantitative proteomic analysis shows differentially expressed HSPB1 in glioblastoma as a discriminating short from long survival factor and NOVA1 as a differentiation factor between low-grade astrocytoma and oligodendroglioma. BMC Cancer 15, 1–13.

Gorabi, A.M., Kiaie, N., Aslani, S., Sathyapalan, T., Jamialahmadi, T., Sahebkar, A., 2021. Implications on the therapeutic potential of statins via modulation of autophagy. Oxid. Med. Cell. Longev. 2021, 1–10.

Gruenbacher, G., Thurnher, M., 2018. Mevalonate metabolism in cancer stemness and trained immunity. Front. Oncol. 8, 394.

Guo, S.-K., Shen, M.-F., Yao, H.-W., Liu, Y.-S., 2018. Enhanced expression of TGFBI promotes the proliferation and migration of glioma cells. Cell. Physiol. Biochem. 49, 1138–1150.

Haga, R.B., Ridley, A.J., 2016. Rho GTPases: regulation and roles in cancer cell biology. Small GTPases 7, 207–221.

Hajiahmadi, S., Lorzadeh, S., Iranpour, R., Karima, S., Rajabibazl, M., Shahsavari, Z., Ghavami, S., 2023. Temozolomide, simvastatin and acetylshikonin combination induces mitochondrial-dependent apoptosis in GBM cells, which is regulated by autophagy. Biology 12, 302.

Han, S.J., Kwon, S., Kim, K.S., 2021. Challenges of applying multicellular tumor spheroids in preclinical phase. Cancer Cell Int. 21, 1–19.

Hu, J., Xie, W., Shang, L., Yang, X., Li, Q., Xu, M., Dou, J., Zhou, Y., Niu, W., Wu, Y., 2017. Knockdown of calponin 2 suppressed cell growth in gastric cancer cells. Tumor Biol. 39, 1010428317706455.

Jiang, P., Mukthavaram, R., Chao, Y., Nomura, N., Bharati, I., Fogal, V., Pastorino, S., Teng, D., Cong, X., Pingle, S., 2014a. In vitro and in vivo anticancer effects of mevalonate pathway modulation on human cancer cells. Br. J. Cancer 111, 1562–1571.

Jiang, P., Mukthavavam, R., Chao, Y., Bharati, I.S., Fogal, V., Pastorino, S., Cong, X., Nomura, N., Gallagher, M., Abbasi, T., 2014b. Novel anti-glioblastoma agents and therapeutic combinations identified from a collection of FDA approved drugs. J. Transl. Med. 12, 1–13.

Jiang, W., Hu, J.-W., He, X.-R., Jin, W.-L., He, X.-Y., 2021. Statins: a repurposed drug to fight cancer. J. Exp. Clin. Cancer Res. 40, 1–33.

Kang, X., Wang, F., Lan, X., Li, X., Zheng, S., Lv, Z., Zhuang, Y., Zhao, Y., Zhou, S., 2018. Lentivirus-mediated shRNA targeting CNN2 inhibits hepatocarcinoma in vitro and in vivo. Int. J. Med. Sci. 15, 69.

Kanzawa, T., Germano, I., Komata, T., Ito, H., Kondo, Y., Kondo, S., 2004. Role of autophagy in temozolomide-induced cytotoxicity for malignant glioma cells. Cell Death Differ. 11, 448–457.

Kim, Y., Varn, F.S., Park, S.-H., Yoon, B.W., Park, H.R., Lee, C., Verhaak, R.G., Paek, S.H., 2021. Perspective of mesenchymal transformation in glioblastoma. Acta neuropathologica communications 9, 1–20.

Kochanowski, P., Catapano, J., Pudełek, M., Wróbel, T., Madeja, Z., Ryszawy, D., Czyż, J., 2021. Temozolomide induces the acquisition of invasive phenotype by o6-methylguanine-dna methyltransferase (Mgmt)+ glioblastoma cells in a snail-1/cx43-dependent manner. Int. J. Mol. Sci. 22, 4150.

Koo, J.H., Guan, K.-L., 2018. Interplay between YAP/TAZ and metabolism. Cell Metabol. 28, 196–206.

Kotecha, R., Odia, Y., Khosla, A.A., Ahluwalia, M.S., 2023. Key clinical principles in the management of glioblastoma. JCO oncology practice 19, 180–189.

Lee, N., Tilija Pun, N., Jang, W.J., Bae, J.W., Jeong, C.H., 2020. Pitavastatin induces apoptosis in oral squamous cell carcinoma through activation of FOXO3a. J. Cell Mol. Med. 24, 7055–7066.

Li, J., Liu, Q., Liu, Z., Xia, Q., Zhang, Z., Zhang, R., Gao, T., Gu, G., Wang, Y., Wang, D., 2018. KPNA2 promotes metabolic reprogramming in glioblastomas by regulation of c-myc. J. Exp. Clin. Cancer Res. 37, 1–15.

Liberti, M.V., Locasale, J.W., 2016. The Warburg effect: how does it benefit cancer cells? Trends Biochem. Sci. 41, 211–218.

Lié, O., Virolle, T., Gabut, M., Pasquier, C., Zemmoura, I., Augé-Gouillou, C., 2022. SETMAR shorter isoform: a new prognostic factor in glioblastoma. Front. Oncol. 11, 638397.

Lv, H., Sun, J.-G., Wang, G.-J., Zhu, X.-Y., Zhang, Y., Gu, S.-H., Liang, Y., Sun, J., 2007. Determination of pitavastatin in human plasma via HPLC-ESI-MS/MS and subsequent application to a clinical study in healthy Chinese volunteers. Clin. Chim. Acta 386, 25–30.

Magalhães, M., Domínguez-Martín, E.M., Jorge, J., Gonçalves, A.C., Díaz-Lanza, A.M., Manadas, B., Efferth, T., Rijo, P., Cabral, C., 2022. Parvifloron D-based potential therapy for glioblastoma: inducing apoptosis via the mitochondria dependent pathway. Front. Pharmacol. 13, 1006832.

Marino, G., Niso-Santano, M., Baehrecke, E.H., Kroemer, G., 2014. Self-consumption: the interplay of autophagy and apoptosis. Nat. Rev. Mol. Cell Biol. 15, 81–94.

Marquez, R.T., Xu, L., 2012. Bcl-2: beclin 1 complex: multiple, mechanisms regulating autophagy/apoptosis toggle switch. Am. J. Cancer Res. 2, 214.

Miranda, A., Blanco-Prieto, M., Sousa, J., Pais, A., Vitorino, C., 2017. Breaching barriers in glioblastoma. Part I: molecular pathways and novel treatment approaches. Int. J. Pharm. 531, 372–388.

Mustafov, D., Karteris, E., Braoudaki, M., 2023. Deciphering the role of microRNA mediated regulation of coronin 1C in glioblastoma development and metastasis. Non-Coding RNA 9, 4.

Ostrom, Q.T., Price, M., Neff, C., Cioffi, G., Waite, K.A., Kruchko, C., Barnholtz-Sloan, J. S., 2022. CBTRUS statistical report: primary brain and other central nervous system tumors diagnosed in the United States in 2015–2019. Neuro Oncol. 24, v1–v95.

Palukuri, M.V., Patil, R.S., Marcotte, E.M., 2023. Molecular complex detection in protein interaction networks through reinforcement learning. BMC Bioinf. 24, 306.

Pang, L., Dunterman, M., Guo, S., Khan, F., Liu, Y., Taefi, E., Bahrami, A., Geula, C., Hsu, W.-H., Horbinski, C., 2023. Kunitz-type protease inhibitor TFPI2 remodels stemness and immunosuppressive tumor microenvironment in glioblastoma. Nat. Immunol. 24, 1654–1670.

Parrales, A., Thoenen, E., Iwakuma, T., 2018. The interplay between mutant p53 and the mevalonate pathway. Cell Death Differ. 25, 460–470.

Peng, P., Wei, W., Long, C., Li, J., 2017. Atorvastatin augments temozolomide's efficacy in glioblastoma via prenylation-dependent inhibition of Ras signaling. Biochem. Biophys. Res. Commun. 489, 293–298.

Pereira, M., Matuszewska, K., Glogova, A., Petrik, J., 2022. Mutant p53, the mevalonate pathway and the tumor microenvironment regulate tumor response to statin therapy. Cancers 14, 3500.

Portnow, J., Badie, B., Chen, M., Liu, A., Blanchard, S., Synold, T.W., 2009. The neuropharmacokinetics of temozolomide in patients with resectable brain tumors: potential implications for the current approach to chemoradiation. Clin. Cancer Res. 15, 7092–7098.

Rapp, M., Baernreuther, J., Turowski, B., Steiger, H.-J., Sabel, M., Kamp, M.A., 2017. Recurrence pattern analysis of primary glioblastoma. World neurosurgery 103, 733–740.

Raza, A., Yen, M.-C., Anuraga, G., Shahzadi, I., Mazhar, M.W., Ta, H.D.K., Xuan, D.T.M., Dey, S., Kumar, S., Santoso, A.W., 2023. Comparative analysis of the gnai family genes in glioblastoma through transcriptomics and single-cell technologies. Cancers 15, 5112.
Rendon, L.F., Tewarie, I.A., Cote, D.J., Gabriel, A., Smith, T.R., Broekman, M.L., Mekary, R.A., 2022. Statins and gliomas: a systematic review of the preclinical studies and meta-analysis of the clinical literature. Drugs 82, 293–310.
Rezazadeh, D., Norooznezhad, A.H., Mansouri, K., Jahani, M., Mostafaie, A., Mohammadi, M.H., Modarressi, M.H., 2020. Rapamycin reduces cervical cancer cells viability in hypoxic condition: investigation of the role of autophagy and apoptosis. OncoTargets Ther. 4239–4247.
Rodríguez-Expósito, R.L., Sifaoui, I., Reyes-Batlle, M., Maciver, S.K., Piñero, J.E., Lorenzo-Morales, J., 2022. Statins induce actin cytoskeleton disassembly and an apoptosis-like process in acanthamoeba spp. Antibiotics 11, 280.
Ryu, H.-H., Jung, S., Jung, T.-Y., Moon, K.-S., Kim, I.-Y., Jeong, Y.-I., Jin, S.-G., Pei, J., Wen, M., Jang, W.-Y., 2012. Role of metallothionein 1E in the migration and invasion of human glioma cell lines. Int. J. Oncol. 41, 1305–1313.
Sahebkar, A., Kiaie, N., Gorabi, A.M., Mannarino, M.R., Bianconi, V., Jamialahmadi, T., Pirro, M., Banach, M., 2021. A comprehensive review on the lipid and pleiotropic effects of pitavastatin. Prog. Lipid Res. 84, 101127.
Seker, F., Cingoz, A., Sur-Erdem, I., Erguder, N., Erkent, A., Uyulur, F., Esai Selvan, M., Gümüş, Z.H., Gönen, M., Bayraktar, H., 2019. Identification of SERPINE1 as a regulator of glioblastoma cell dispersal with transcriptome profiling. Cancers 11, 1651.
Seystahl, K., Tritschler, I., Szabo, E., Tabatabai, G., Weller, M., 2015. Differential regulation of TGF-β–induced, ALK-5–mediated VEGF release by SMAD2/3 versus SMAD1/5/8 signaling in glioblastoma. Neuro Oncol. 17, 254–265.
Shojaei, S., Alizadeh, J., Thliveris, J., Koleini, N., Kardami, E., Hatch, G., Xu, F., Hombach-Klonisch, S., Klonisch, T., Ghavami, S., 2018. Inhibition of autophagy by mevalonate pathway inhibitors, a new therapeutic approach to sensitize glioblastoma cells to temozolomide induced apoptosis. Faseb. J. 32, 533.541, 533.541.
Sidaway, P., 2017. Glioblastoma subtypes revisited. Nat. Rev. Clin. Oncol. 14, 587, 587.
Sodek, K.L., Brown, T.J., Ringuette, M.J., 2008. Collagen I but not Matrigel matrices provide an MMP-dependent barrier to ovarian cancer cell penetration. BMC Cancer 8, 1–11.
Steponaitis, G., Tamasauskas, A., 2021. Mesenchymal and proneural subtypes of glioblastoma disclose branching based on gsc associated signature. Int. J. Mol. Sci. 22, 4964.
Stupp, R., Mason, W.P., Van Den Bent, M.J., Weller, M., Fisher, B., Taphoorn, M.J., Belanger, K., Brandes, A.A., Marosi, C., Bogdahn, U., 2005a. Radiotherapy plus concomitant and adjuvant temozolomide for glioblastoma. N. Engl. J. Med. 352, 987–996.
Stupp, R., Mason, W.P., Van Den Bent, M.J., Weller, M., Fisher, B., Taphoorn, M.J.B., Belanger, K., Brandes, A.A., Marosi, C., Bogdahn, U., 2005b. Radiotherapy plus concomitant and adjuvant temozolomide for glioblastoma. N. Engl. J. Med. 352, 987–996.
Tang, Z., Kang, B., Li, C., Chen, T., Zhang, Z., 2019. GEPIA2: an enhanced web server for large-scale expression profiling and interactive analysis. Nucleic Acids Res. 47, W556–W560.
Verhaak, R.G., Hoadley, K.A., Purdom, E., Wang, V., Qi, Y., Wilkerson, M.D., Miller, C.R., Ding, L., Golub, T., Mesirov, J.P., 2010. Integrated genomic analysis identifies clinically relevant subtypes of glioblastoma characterized by abnormalities in PDGFRA, IDH1, EGFR, and NF1. Cancer Cell 17, 98–110.
Vinci, M., Gowan, S., Boxall, F., Patterson, L., Zimmermann, M., Court, W., Lomas, C., Mendiola, M., Hardisson, D., Eccles, S.A., 2012. Advances in establishment and analysis of three-dimensional tumor spheroid-based functional assays for target validation and drug evaluation. BMC Biol. 10, 1–21.
Vollmann-Zwerenz, A., Leidgens, V., Feliciello, G., Klein, C.A., Hau, P., 2020. Tumor cell invasion in glioblastoma. Int. J. Mol. Sci. 21, 1932.
Wang, M., Zhang, C., Zheng, Q., Ma, Z., Qi, M., Di, G., Ling, S., Xu, H., Qi, B., Yao, C., 2022a. RhoJ facilitates angiogenesis in glioblastoma via JNK/VEGFR2 mediated activation of PAK and ERK signaling pathways. Int. J. Biol. Sci. 18, 942.
Wang, Q., Hu, B., Hu, X., Kim, H., Squatrito, M., Scarpace, L., DeCarvalho, A.C., Lyu, S., Li, P., Li, Y., 2017a. Tumor evolution of glioma-intrinsic gene expression subtypes associates with immunological changes in the microenvironment. Cancer Cell 32, 42–56. e46.
Wang, X., Huang, Z., Wu, Q., Prager, B.C., Mack, S.C., Yang, K., Kim, L.J., Gimple, R.C., Shi, Y., Lai, S., 2017b. MYC-regulated mevalonate metabolism maintains brain tumor–initiating cells. Cancer Res. 77, 4947–4960.
Wang, Z., Mo, Y., Tan, Y., Wen, Z., Dai, Z., Zhang, H., Zhang, X., Feng, S., Cheng, Q., 2022b. The ALDH family contributes to immunocyte infiltration, proliferation and epithelial-mesenchymal transformation in glioma. Front. Immunol. 12, 756606.
Weis, M., Heeschen, C., Glassford, A.J., Cooke, J.P., 2002. Statins have biphasic effects on angiogenesis. Circulation 105, 739–745.
Wen, S., Tu, X., Zang, Q., Zhu, Y., Li, L., Zhang, R., Abliz, Z., 2024. Liquid chromatography–mass spectrometry-based metabolomics and fluxomics reveals the metabolic alterations in glioma U87MG multicellular tumor spheroids versus two-dimensional cell cultures. Rapid Commun. Mass Spectrom. 38, e9670.
Xiao, A., Brenneman, B., Floyd, D., Comeau, L., Spurio, K., Olmez, I., Lee, J., Nakano, I., Godlewski, J., Bronisz, A., 2019. Statins affect human glioblastoma and other cancers through TGF-β inhibition. Oncotarget 10, 1716.
Yan, H., Parsons, D.W., Jin, G., McLendon, R., Rasheed, B.A., Yuan, W., Kos, I., Batinic-Haberle, I., Jones, S., Riggins, G.J., Friedman, H., Friedman, A., Reardon, D., Herndon, J., Kinzler, K.W., Velculescu, V.E., Vogelstein, B., Bigner, D.D., 2009. IDH1 and IDH2 mutations in gliomas. N. Engl. J. Med. 360, 765–773.
You, H.-Y., Zhang, W.-J., Xie, X.-M., Zheng, Z.-H., Zhu, H.-L., Jiang, F.-Z., 2016. Pitavastatin suppressed liver cancer cells in vitro and in vivo. OncoTargets Ther. 5383–5388.
Yuan, Z., Li, Y., Zhang, S., Wang, X., Dou, H., Yu, X., Zhang, Z., Yang, S., Xiao, M., 2023. Extracellular matrix remodeling in tumor progression and immune escape: from mechanisms to treatments. Mol. Cancer 22, 48.
Zahedipour, F., Butler, A.E., Rizzo, M., Sahebkar, A., 2022. Statins and angiogenesis in non-cardiovascular diseases. Drug Discov. Today 27, 103320.
Zhao, M., Tan, B., Dai, X., Shao, Y., He, Q., Yang, B., Wang, J., Weng, Q., 2019. DHFR/TYMS are positive regulators of glioma cell growth and modulate chemo-sensitivity to temozolomide. Eur. J. Pharmacol. 863, 172665.
Zhao, W., Li, X., Nian, W., Wang, J., Wang, X., Sun, L., Zhu, Y., Tong, Z., 2021. Ribosome proteins represented by RPL27A mark the development and metastasis of triple-negative breast cancer in mouse and human. Front. Cell Dev. Biol. 9, 716730.
Zhao, W., Wu, Y., Wang, S., Zhao, F., Liu, W., Xue, Z., Zhang, L., Wang, J., Han, M., Li, X., 2024. HTRA1 promotes EMT through the HDAC6/Ac-α-tubulin pathway in human GBM cells. CNS Neurosci. Ther. 30, e14605.
Zhu, Z., Zhang, P., Li, N., Kiang, K.M.Y., Cheng, S.Y., Wong, V.K.-W., Leung, G.K.-K., 2019. Lovastatin enhances cytotoxicity of temozolomide via impairing autophagic flux in glioblastoma cells. BioMed Res. Int. 2019, 2710693.